MODELING OF WAVE IMPACT USING A PENDULUM SYSTEM

A Thesis

by

CHUNYONG NIE

Submitted to the Office of Graduate Studies of
Texas A&M University
in partial fulfillment of the requirements for the degree of

MASTER OF SCIENCE

May 2010

Major Subject: Ocean Engineering

MODELING OF WAVE IMPACT USING A PENDULUM SYSTEM

A Thesis

by

CHUNYONG NIE

Submitted to the Office of Graduate Studies of
Texas A&M University
in partial fulfillment of the requirements for the degree of

MASTER OF SCIENCE

Approved by:

Chair of Committee,	John M. Niedzwecki
Committee Members,	Jun Zhang
	H. Joseph Newton
Head of Department,	John M. Niedzwecki

May 2010

Major Subject: Ocean Engineering

ABSTRACT

Modeling of Wave Impact Using a Pendulum System. (May 2010)

Chunyong Nie, B.S., Harbin Engineering University

Chair of Advisory Committee: Dr. John M. Niedzwecki

For high speed vessels and offshore structures, wave impact, a main source of environmental loads, causes high local stresses and structural failure. However, the prediction of wave impact loads presents numerous challenges due to the complex nature of the instant structure-fluid interaction. The purpose of the present study is to develop an effective wave impact model to investigate the dynamic behaviors of specific shaped elements as they impact waves. To achieve this objective, a wave impact model with a body swinging on a pendulum system is developed. The body on the pendulum goes through a wave free surface driven by gravity at the pendulum's natural frequency. The system's motion and impact force during the entire oscillation time beginning from the instant of impact are of interest. The impact force is calculated by applying von Karman's method, which is based on momentum considerations. The usual wave forces are presented in the Morison's equation and incorporated into dynamic systems with other wave forces. For each body shape, the dynamic system is described by a strongly nonlinear ordinary differential equation and then solved by a Runge-Kutta differential equation solver. The dynamic response behavior and the impact force time history are obtained numerically and the numerical results show support the selection of a pendulum

model as an efficient approach to study slamming loads. The numerical prediction of this model is compared to previous experiments and classification society codes.

Moreover, a basic design of wave impact experiments using this pendulum model is proposed to provide a more accurate comparison between numerical results and experimental data for this model. This design will also serve as a first look at the experimental application of the pendulum model for the purpose of forecasting slamming force.

DEDICATION

To my family

ACKNOWLEDGEMENTS

This research study was supported by the Texas Engineering Experiment Station and the R.P.Gregory ’32 Chair Endowment. Each of these funding sources is gratefully acknowledged.

I would like to express my gratitude and thanks to my advisor, Dr. John M. Niedzwecki, for his enlightening guidance on my understanding of the study and enormous contribution to my academic pursuits. I would also like to thank my advisory committee members: Dr. H. Joseph Newton and Dr. Jun Zhang, for their trust and guidance throughout this research project.

Thanks also go to my friends and colleagues and the department faculty and staff for making my time at Texas A&M University a great experience

Finally, thanks to my mother and father, as well as my girlfriend, for their encouragement and support.

TABLE OF CONTENTS

Page

Page

LIST OF FIGURES

Page

Page

Page

Page

LIST OF TABLES

Page

1. INTRODUCTION

One important objective of research in offshore engineering is to develop methods of designing safe and economic structures. The prediction of operational and extreme loads caused by the environmental forces is of particular interest to designers of offshore structures and ships. Naval architects are concerned with ships underway slamming into waves and in particular the impact occurring with the ship moving with relatively high forward speed. These slamming impact loads result in localized high pressure on the hull. If these slamming loads occur with high frequency, it may lead to structural fatigue problems, especially for high speed vessels.

Faltinsen (1990) defined slamming impact as 'impulse loads with high pressure peaks occur during impact between a body and water'. There are several types of ship slamming in practice. Slamming on a bow flare or bottom occurs in rough seas, when the ship is lifted out of water and enters the water again. The slamming impact also happens on vertical columns or horizontal structural members in the splash zone on offshore platforms, usually in the presence of wave breaking. Wet-deck slamming acts on the bottom of the platform deck or the catamaran deck connecting the two pieces, when the heave motion is large. Green water slamming occurs on the bow stem by breaking waves or on the upper deck and bridge in rough seas when incoming waves run-up on a floating platform and exceed the freeboard. Green water used to be exclusively a topic for high speed ships, but it is now of concern for offshore ship structures like Floating Production, Storage and Offloading Systems (FPSO), where no operational measures can be applied to reduce green water like voluntary speed reduction. For vessels with liquid tank onboard, slamming acts on the inner side of a partially filled tank, and results in sloshing loads.

Behind the diversity of slamming impact in outward forms, there is some common ground underlying in the physics of slamming. The most essential action during slamming is that a body enters the water free surface, named water entry. Water entry appears to be the most popular slamming model as it is used by many researchers, von

---

This thesis follows the style of Ocean Engineering.

Karman (1929), Wagner (1932), Faltinsen (1977), Campbell & Weyberg (1980), R. Zhao (1993), etc. During slamming, wave breaking can release large amount of energy on vertical or inclined cylindrical structural members. Water run-up along columns may cause damage on platform decks during slamming. When slamming occurs, the wave impact force dominates the more usual wave induced hydrodynamic forces and buoyancy loading.

1.1. Literature review

Slamming is a complicated nonlinear physical process, where jet flow, air trapping, and water compressibility may be involved. The classic simplified analytical formula for water impact cannot adequately take these factors into account. With the advancement of computational capability, more accurate solutions have obtained and the prediction of various wave impact loads now compare more favorably with experiment results.

Analytical methods developed for the water entry of simple shapes have a long history. The pioneering analytical methods were established by von Karman (1929) and Wagner (1932). Von Karman's method is based upon momentum considerations. The momentum of the fluid-body system increases during impact because the hydrodynamic added-mass occurs, such that the system momentum after penetration must be equal to the sum of the body momentum and hydrodynamic added-mass momentum. More specifically, in Wagner's method, the velocity potential is first found from the solution of the boundary value problem for a 2-dimension plane, and then the impact pressure is determined from Bernoulli's equation. Wagner's method accounts for local free surface elevation and thus has been found to yield conservative estimation of peak impact pressures, while von Karman's method tends to underestimate impact force. Kaplan and Silbert (1976) applied von Karman's method to a horizontal cylinder and investigated the process from wave impact through fully submerged status. They considered the wave impact force as a sum of the buoyant force, the time-rate of the change of hydrodynamic added-mass momentum and the dynamic pressure due to surface oscillation. The

hydrodynamic added-mass was expressed using Taylor's cylinder added-mass formula that allowed them to obtain the derivative of the added-mass analytically. Sarpkaya (1978) further improved von Karman's analytical solution. He found that it was not realistic to assume that slamming coefficients reached a maximum value instantaneously at t=0. Thus, a model of rise time was introduced which allowed a finite time for the slamming coefficient to reach its maximum. He assumed the slamming coefficient increases linearly during the rise time, and set different values to the rise time. Sarpkaya also proposed the global dynamic response transfer function of rigid cylinders. The transfer function was found to be very sensitive to the duration of rise time assumed, i.e., when the rise time was larger than 1/100 sec, the transfer function dramatically lost its harmonic shape. Isaacson and Prasad (1994) investigated the wave impact loads due to waves interacting with a horizontal cylinder near the free surface. A single degree of freedom dynamic model was established using slamming coefficients and other hydrodynamic coefficients from experimental data. The time history of the vertical impact force and dynamic response of the cylinder was obtained by solving the differential equation numerically by using a time-stepping procedure. Korobkin (1996) presented acoustic approximation and a method of normal modes to study the defection of a curved plate under slamming and included the effect of weak fluid compressibility. Bifurcation analysis on the nonlinear dynamics system excited by slamming was introduced by Liaw et al. (1996) and the bifurcation behavior of a horizontal cylinder under water slamming was proven not sensitive to the magnitude of the slamming force. Oliver (2007) developed a second order correction of Wagner's method for the location of the high pressure on the jet-root region and the upward force. The solution of an entering wedge using the correction was compared well with experimental and numerical results.

Unlike analytical methods, numerical methods can be used to more accurately address complex shapes of practical interest. The most developed numerical method for slamming problems is the Boundary Element Method (BEM). Zhao et al. (1993) presented nonlinear BEM to solve water entry of arbitrary cross section neglecting the

consideration of jet flow. Their results compared favorably with experimental results. In 1997, Zhao developed two methods in water entry of arbitrary 2-D section. The first method is a fully nonlinear numerical simulation, and flow separation was considered. The second method was an approximate approach, extending Wagner's classical method, but not including flow separation. The latter is a very robust numerical method, referred to as the 'Generalized Wagner method', where the body-boundary conditions with a free surface approximation are applied in Wagner's outer flow domain. The results were validated by using vessel cross-sections and dropping them into an initially quiescent fluid. Hermundstad & Moan (2005) applied nonlinear strip theory and Wagner's method to investigate slamming impacts of a vessel with BEM codes. The 3-D numerical results compared well with experimental results. Greco et al. (2008) investigated the bottom slamming a Very Large Floating Structure using a boundary element method. Linear global analysis and nonlinear local analysis for platform behavior without coupling global and local analysis was studied separately.

In addition to Boundary Element method, other methods including the Finite Element Method (FEM) and the Smoothed Particle Hydrodynamics (SPH) method have been used to predict slamming loads. Le Sourne et al. (2003) generally discussed the application of LS-DYNA 3D in slamming simulation, which is a nonlinear dynamics FEM software. Peseux (2005) dealt with slamming between a ship bow and water free surface by solving the 3-D Wagner problem utilizing with the Finite Element Method. The numerical prediction was confirmed by experimental data. Oger et al (2006) used the SPH method for solid-fluid coupling in surface flow context and simulated two wedge water entry problems. Aquelet et al (2006) solved Navier-Stokes equations with an Arbitrary Lagrangian Eulerian (ALE) formulation for the fluid and a Lagrange formulation for the structure to predict impact loads on a wedge shape entering an undisturbed fluid. Chen (2009) used a computational fluid dynamics method to solve the unsteady Navier-Stokes equations with an interface-preserving level-set method for the simulation of green water effect on offshore structures and ships.

Despite the sophisticated development of numerical methods, the slamming problem is still too difficult to be modeled completely due to its short time scale and complication when considering a random wave field. Thus experimental methods remain a strong component of wave slamming research. Faltinsen (1977) conducted an experiment of horizontal Polyvinyl Chloride (PVC) cylinders to simulate the slamming on trusses of semisubmersibles. The pinned-end horizontal PVC cylinders were forced with constant velocities through an initially undisturbed free surface. The results of the tests were found to be up to 100% higher than the theoretical prediction. The slamming coefficients obtained from the tests had an average of 5.3, as compared to theoretical value at 3.1.

Sarpkaya (1978) conducted the experiments in a U-shaped water tunnel with two vertical legs which could initiate oscillations of free surface. Horizontal rough aluminum cylinders supported elastically were tested in one of the legs. An accelerometer was placed inside each cylinder and impact forces were measured by wave transducers attached to the cylinders. The measured initial slamming coefficient was found close to theoretical value π. The experiment showed that the dynamic response was as important as the impact force. The slamming coefficient can be amplified or attenuated to the initial value according to the dynamic system characteristics. It was also found that the drag force becomes important after the cylinders are the fully submerged.

Suchithra et al. (1995) conducted a series of laboratory tests of wave impact on horizontal plates with and without stiffeners in a wave flume that was 3m in width and 10m in length, and equipped with a hinged paddle wave maker. He designed a U-shaped aluminum cell to measure axial and bending force. First, waves were generated without the slab and with the wave probe at the intended location of the slab. Then the wave probe was removed and the slab was placed at the designed location. The factors affecting slamming coefficients were discussed, including wave frequency, deck clearance, the presence of stiffeners, and Keulegan-Carpenter number.

Yoshimoto et al. (1997) conducted experiments to estimate the bottom slamming loaded on a pontoon-type very large floating structure model scaled with the ratio of

1:37.5. The models were made from aluminum honeycomb panels with the purpose of easily manufacturing the target rigidity. The vertical movement of the vessels was measured using LED lights and there were 10 pressure sensors were attached along the length of each model. Comparison between two models with different mattering rigidity in materials was presented. The results indicated the model with low rigidity had smaller extent of bottom emergence but larger impact pressure.

Hermundstad and Moan (2005) conducted model tests for the slamming on the bow flare of a Ro-Ro ship with P-P length of 120 m and service speed of 20 knots. The model with scale ratio 1:21.62 was self-propelled with only cable and rope connected it to the carriage. Two slamming panels were amounted on the force transducers to measure the impact pressure. The ship motion was measured using an optical system. The tests were conducted in different wave headings at the heave/pitch resonance period. The results of the tests agreed well with the numerical results obtained from existing Boundary Element Method software.

Table 1, 2 and 3 summarize the previous studies on wave impact.

Table 1. Selected important papers using analytical methods for slamming problems

Year	Author	Paper title	Brief overview
1932	H. Wagner	Uber Stossund Gleitvorgange an der Oberflache von Flussigkeiten	A water impact theory was derived with consideration of free surface elevation. The theory can be applied to arbitrary shape with small deadrise angle. Although air trap and compressibility isn't included, the theory is still strong even today, because it can be used to accurately present impact pressure and it is a conservative method in practice.
1976	Kaplan and Silbert	Impact Forces on Horizontal members in the splash zone	A solution for a cylinder from impact starting instant to full immersion in wave has been obtained. The force acting on the cylinder is considered as the sum of buoyancy and the rate of change of momentum which is related to the wave elevation.
1996	Korobkin	Acoustic approximation in the slamming problem	A solid, slightly curved plate impact on weak compressible water has been investigated using acoustic approximation and the method of normal modes. The supersonic stage during the impact when the free surface remains undisturbed outside the contact position is concerned. The comparison between rigid body impact and elastic boy impact is made.
2007	Oliver	Second-order Wagner theory for two-dimensional water-entry problems at small deadrise angles	The second-order corrections of Wagner's theory have been made for the jet-root regions and the upward force on the structure. The results are compared with numerical and experimental data. The prediction capability of Wagner's theory is improved.

Table 2. Selected important papers using numerical methods for slamming problems

Year	Author	Paper title	Brief overview
1987	Greenhow	Wedge entry into initial calm water	A versatile numerical approach has been introduced concerning wedges of various angles entry initial calm water with both gravity and the nonlinearity of the boundary conditions on the wedge and free surfaces taken into account for the first time.
1993	Zhao et al.	Water entry of two dimensional body	Nonlinear BEM has been presented to solve water entry of arbitrary cross section without the consideration of jet flow. The results were compared with experimental results. For small deadrise angles the results agree well with Wagner's theory.
1997	Zhao et al.	Water entry of arbitrary two-dimensional sections with and without flow separation	Two methods have been developed for arbitrary two-dimensional sections slamming problem. One is a nonlinear BEM numerical simulation approach taking flow separation into account. The other is a generalization of Wagner's method without flow separation. The results of this method agree with the nonlinear method and the calculation is efficient.
2006	G. Oger et al	Two-dimensional SPH simulations of wedge water entries	The smoothed particles hydrodynamics method (SPH) has been introduced for a numerical simulation for solid-fluid impact on a free surface. Two wedge water entry cases are simulated and results are compared with analytical and experimental data to validate the new numerical method.
2008	Greco et al	Bottom slamming for a Very Large Floating Structure: Uncoupled global and slamming analyses	The bottom slamming for a very large floating structure (VLFS) has been studied. Linear analysis for global motion and nonlinear analysis for flow evolution and local stresses without flow separation. The coupling between global behavior and local phenomena is not taken into account. The hydroelastic coupling and air cushion associated with scale transferring challenges are discussed.

Table 3. Selected important papers using experimental methods to investigate slamming problems

Year	Author	Paper title	Brief overview
1977	Faltinsen	Water impact loads and dynamic response of horizontal circular cylinders in offshore structures	Experiments of rigid horizontal cylinder and horizontal elastic cylinder have been conducted respectively. The experimental results are both larger than theoretic results. For realistic extreme wave conditions in the North Sea, the stresses could be higher than yield stress according to the model results.
1978	Sarpkaya	Wave impact loads on cylinders	Slamming experiments of a horizontal cylinder under impact of harmonically oscillating flow has been conducted. The experiments focused on the dynamic response of system, the dynamic characteristics, the slamming coefficient, and the effect of drag force. It validated the theoretical value of slamming coefficient at initial time is π, and showed that it lies between 0.5π and 1.7π related to the rise time and natural frequency of the cylinder.
1995	Suchithra et al.	A study of wave impact on horizontal slabs	A laboratory study of wave impact on horizontal slabs has been conducted, and slamming coefficients under different conditions has been examined. The effect of stiffener arrangement, wave frequency, deck clearance were investigated. Freak waves were also investigated with regards to the wave impact .
1997	Yoshimoto et al	Slamming load on a very large floating structure with shallow draft	Experiments have been conducted to estimate the bottom slamming load on a pontoon-type very large floating structure with a shallow draft. The models were made from aluminum honeycomb panels. The scaling ratio of models is 1:37.5. The results are related to a simple analytical method.
2005	Hermundstad & Moan	Numerical and experimental analysis of bow flare slamming on a Ro-Ro vessel in regular oblique waves	A method to predict the slamming load on a Ro-Ro hull is introduced using nonlinear strip theory and generalized Wagner's theory. BEM is used to solve the equations. Model test of the hull is conducted in regular wave of different directions and heights The results of experiments and numerical solutions agree well.

1.2. Research objectives

Slamming impact on structures of different shapes has been studied with various methods, including some very accurate numerical schemes and software implementations. With existing codes, the impact pressure distribution can be obtained and generally agrees well with the experimental data. However, most of the research has focused on the hydrodynamic loading. Some studies have considered local behavior and reliability under slamming, but only a few of them have investigated the dynamic behavior of the system due to wave impact. The existing experimental studies have focused on either the simple structure or the ship model tests. However, the ship model tests are costly and due to scale effects, it may be questionable to apply the experimental findings of one ship model to other ship forms. The slamming tests of simple shapes are mostly for fixed structures or structures forced at certain velocities, and thus can't adequately account for the dynamic behavior of the floating or compliant structures.

A basic objective of this thesis research is to investigate the global response of the nonlinear slamming dynamics of specific shaped elements impacting with waves. To achieve this objective, wave impact on a body swinging on a pendulum system, which is similar to realistic wave impact encountered by ships and ocean structural elements, is investigated. The body on the pendulum goes through wave free surface driven by gravity at the pendulum's natural frequency. The system motion and impact force during the whole oscillating time history starting from the impact instant is of interest.

An analytical model to be used as the basis for the numerical simulation to study wave impact on pendulum systems will be presented. A variety of elementary body shapes swinging on the pendulum into an oncoming wave are investigated. Linear stretching wave theory is used to obtain values of pressure distribution and particle motion on each point at the interface. Using stretching wave theory, the relative position between free surface and the body can be evaluate more actually than in previous research studies (Isaacson 1994). Gravity acts as the major restoring force of the system, while the hydrodynamic forces correspond to the exciting force acting on the system. The hydrodynamic force on various body shapes being tested consists of drag force, the

Froude-Krylov force and the actual impact force. The hydrostatic force is calculated based upon Archimedes principle. Wave diffraction and radiation during the impact and when the object goes beneath the wave free surface is also investigated but not explicitly evaluated included in the numerical computation. Some hydrodynamic parameters obtained from earlier research will be used with von Karman's theoretical model and the nonlinear ordinary differential equations of motion will be solved using a MATLAB time-marching solver. Thus the time history of pendulum/body motion and its impulsive loading history will be obtained. These simulation results will then be compared with experimental data and classification society rules.

2. THEORETICAL ANALYSIS

The prediction of impact loading and structural response of marine structures is of significant importance to ensure the survival of structures in a rough ocean environment. Developing appropriate physical models of wave impact requires a careful review and understanding of each factor that affects wave impact force and the motion of the structures. So it is important to establish a proper physical understanding of the process，such that the analytical models can take into account for as much of this understanding as possible in order to make sure the solutions are realistic and yet solvable.

2.1. Morison wave force on a pendulum system

2.1.1. Stretching wave theory

In the real world, ocean waves are random. However, for the engineering purposes, there are a number of ways to describe ocean waves and their kinematics. One approach is to develop an idealized model for the extreme effects of the random waves based upon a design wave approach. These analytical wave theories provide deterministic expressions for wave kinematics needed for estimating the wave forces. Figure 1 illustrates the region of application for the various wave theories used in offshore design.

Canonical linear wave theory is based on small amplitude assumption that eliminates the second order terms in the free surface boundary conditions, and consequently it is unable to calculate the motion of water particles about static water level (SWL). However, the wave amplitude has significant influence on the wave force and cannot be ignored. The wave stretching method that was first proposed by Wheeler (1969) modifies linear wave theory to enable to account for free surface effects without requiring one use higher order wave theory. Wave stretching methods allow one to estimate the wave kinematics in the water columns that is form the seafloor to the instantaneous wave surface elevations. Wave kinematics can be considered to be

functions of the ratio between vertical position with respect to the seafloor and the distance from free surface to water bottom.

Chakrabarti (2005) developed linear stretching formulas which are quite similar to Wheeler's and give exactly the same value of horizontal particle velocity at free surface, while Chakrabarti's formulas are simpler in expression. Chakrabarti's linear stretching formulas are given by:

$$u = \frac{gkH}{2\omega}\frac{\cosh k(y+d)}{\cosh k\left(d+\eta\right)}\cos\left[k\left(x-ct\right)\right] \tag{1}$$

$$v = \frac{gkH}{2\omega}\frac{\sinh k(y+d)}{\cosh k\left(d+\eta\right)}\sin\left[k\left(x-ct\right)\right] \tag{2}$$

$$\dot{u} = \frac{gkH}{2}\frac{\cosh k(y+d)}{\cosh k\left(d+\eta\right)}\sin\left[k\left(x-ct\right)\right] \tag{3}$$

$$\dot{v} = -\frac{gkH}{2}\frac{\sinh k(y+d)}{\cosh k\left(d+\eta\right)}\cos\left[k\left(x-ct\right)\right] \tag{4}$$

$$p = \rho g\frac{H}{2}\frac{\cosh k(y+d)}{\cosh k\left(d+\eta\right)}\cos\left[k\left(x-ct\right)\right] \tag{5}$$

These equations will be used to describe the wave kinematics in the numerical simulation of wave impact models for this research investigation.

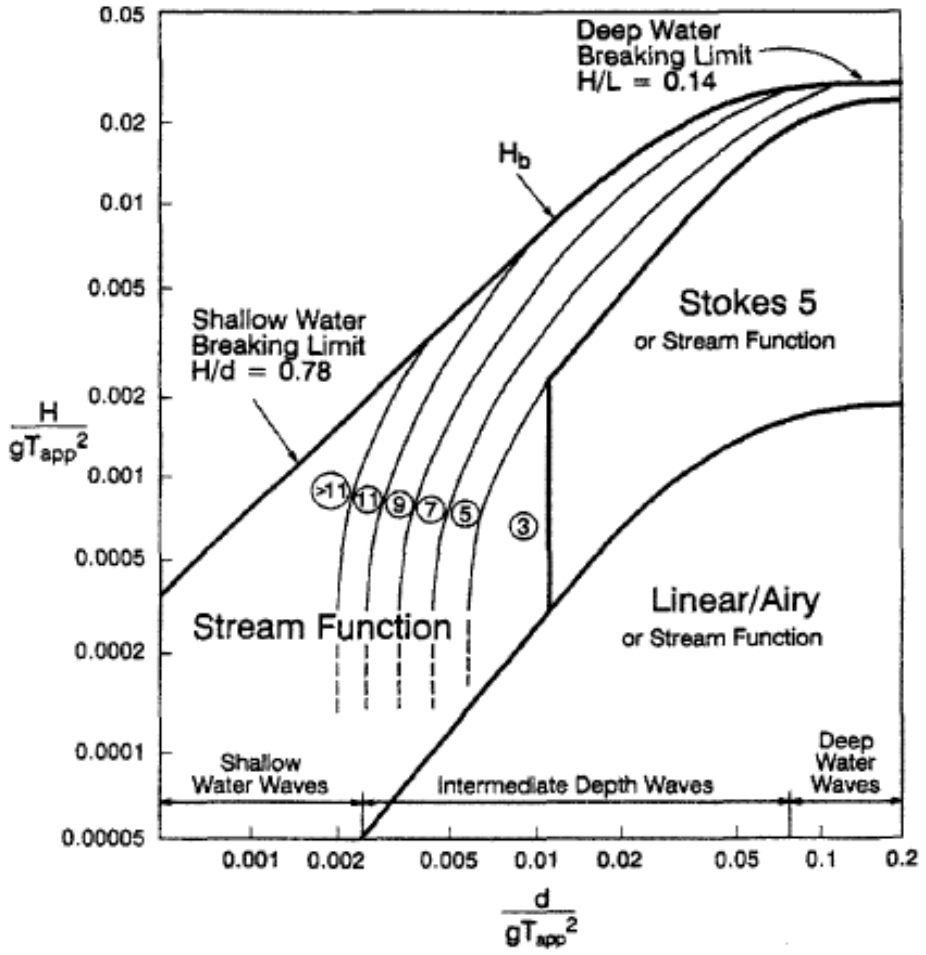

Figure 1. Application range of wave theories (API 2000)

2.1.2. Pendulum system

A pendulum system subjected to wave impact is investigated in this research study, and is illustrated in Figure 2. Similar to an articulated floating system in practice, the pendulum subjected to wave forces can be considered as a single degree of freedom (SDF) system in terms of angular motion:

$$I\ddot{\theta} + C_\theta\dot{\theta} + K_\theta\theta = M \tag{6}$$

where, I is moment of inertia; C_θ and K_θ are angular damping and stiffness coefficients. The exciting force on the RHS can be calculated by diffraction theory. The damping item for offshore platforms is mainly drag force, but there are other resources of damping, like radiation, second-order wave drift and linear viscosity. M is the moment due to wave forces.

In this study, the wave forces other than impact force are evaluated by Morison's equation. When the characteristic dimension, D, of the object is small compared to the wave length λ, the wave force can be evaluated using the Morison equation which can be expressed as:

$$F(t) = \frac{1}{2}\rho C_d A|u_r|u_r + \rho C_m V\frac{du}{dt} \tag{7}$$

where, u is the flow velocity, the relative velocity $u_r = u - \dot{x}$, V is the volume in the water, C_d is the drag coefficient, C_m is the inertia force coefficient. $C_m = C_a + 1$, where C_a is added-mass coefficient. The added-mass is associated with the relative velocity between fluid and structure. In this study, the added-mass coefficients are obtained from previous experimental studies (See Figure 3). In fact, the inertia force in Morison equation is the asymptotic expression of the exact solution from diffraction theory when D/λ is 0.

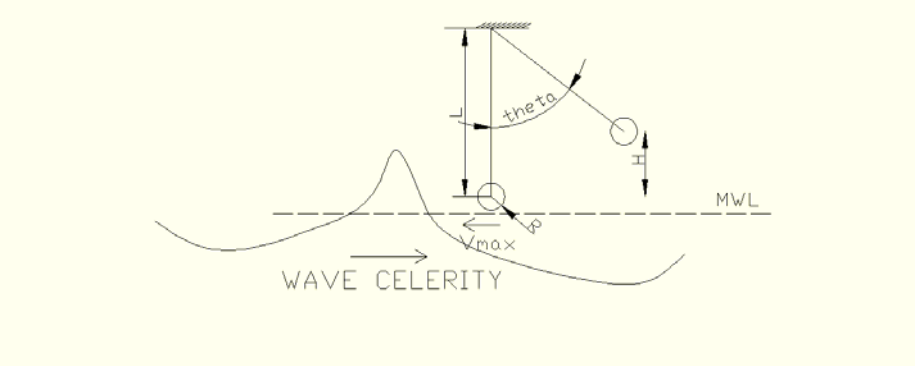

Figure 2. A pendulum system subjected to wave impact

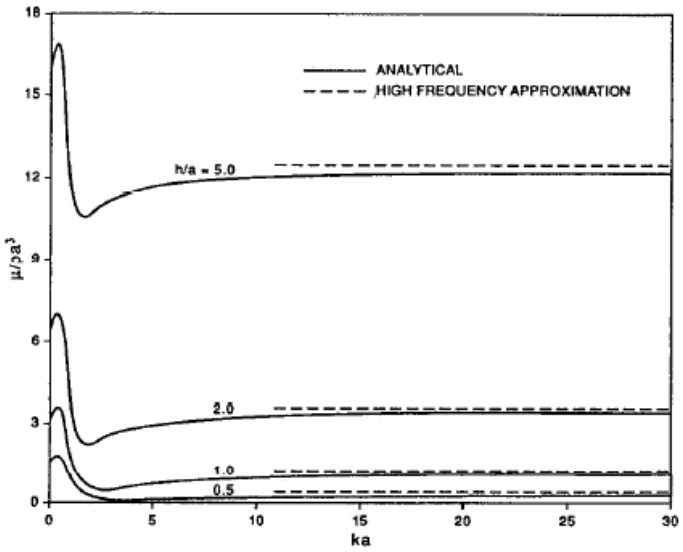

Figure 3. Analytical dimensional added-mass for vertical cylinders. Rahman & Bahtta (1993)

The drag force in the Morison's equation makes the dynamic system nonlinear and this is expressed by the following equation:

$$M_d = \frac{1}{2}\rho C_D A_p \left| l\dot{\theta} - \omega \right| \left(l\dot{\theta} - \omega \right) l \tag{8}$$

where, ω is tangential velocity of water particle $\omega = u\cos\theta - v\sin\theta$. Sarpkaya (1981) provided an analytical method to linearize the drag force, with assumption that radiation damping and exciting moment are linear.

The calculation of usual wave force (not impact) strongly depends on the scale of the objects relative to the scale of wave profiles. Two dimensionless parameters associated with the scale ratio between objects and waves are Keulegan-Carpenter number and scatter parameter.

$$KC = \frac{uT}{D} \tag{9}$$

where, k is wave length; T is wave period; u is water particle velocity; D is characteristic body scale (diameter). And, Scatter parameter = kD. Table 4 illustrates the effects of the scale parameters on wave force estimation. Simply, a diffraction coefficient is defined as the ratio of diffraction force and Froude-Krylov force

$$C_h = \frac{F_{diffraction}}{F_{F-K}} \tag{10}$$

Boccotti (2000) provided the diffraction coefficients for vertical cylinders of different relative radii (see Figure 3) from analytical solutions and tests. The values of both vertical and horizontal diffraction coefficients are about 2. Chakrabarti (1987) also suggested 2.0 as the diffraction coefficient when ka is between 0 and 1.0 for horizontal cylinders.

Radiation effect is that when the body oscillates in the water, the body motion will force or radiate waves. As a result, the velocity potential in the wave field changes as well as the pressure distribution on the body surface. Both radiation and diffraction effects have to be taken into account for oscillating large structures. A significant difference between wave diffraction and wave radiation is that wave diffraction only

contributes to inertia forces but wave radiation contributes to both added-mass and damping. Besides radiation, damping is also from wave drift induced additional resistance and drag. For structure with small underwater part, radiation damping is not significant. Existing programs based on diffraction theory can be used to obtain added-mass and damping coefficients due to radiation. We can simply use data from some analytical and experimental results to estimate the radiation damping coefficients in the pendulum systems (see Figure 4).

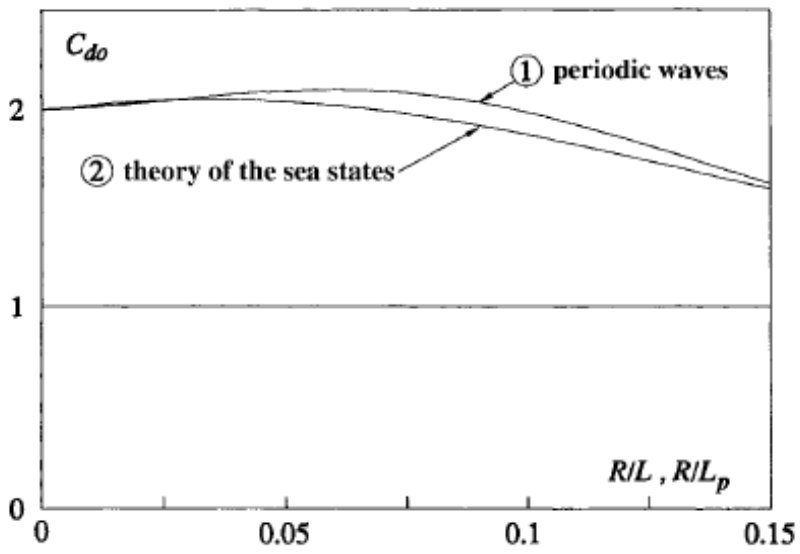

Figure 4. Solutions of diffraction coefficients for vertical cylinders given by Boccotti (2000)

Table 4. Effects of relative body scale on wave force calculation

	KC number<<1	KC number≥1
ka<<1	✓ drag force not important ✓ diffraction not important ✓ Morison equation ✓ Steel jacket structure in operational sea	✓ drag force dominating ✓ diffraction not important ✓ Morison equation ✓ Steel jacket structure in storm sea
ka≥1	✓ Linear diffraction theory ✓ drag force not important ✓ Large floating structure in operational sea	✓ nonlinear diffraction theory ✓ drag force important ✓ formation of vortices ✓ model tests ✓ Large floating structure in storm sea

2.2. Theoretical model for wave impact force

2.2.1. Von Karman's method

The case of initial calm surface entry, first calculated by von Karman (1929), is used as an essential idealization for water impact problems. Faltinsen (1990) investigated a horizontal jacket cylinder truss in the splash zone by using the water entry model and von Karman's method neglecting the wave forces as a first approximation. Von Karman's method is derived by momentum considerations with the assumption of incompressible potential flow.

From a Lagrangian view, the momentum of a group of fluid particle or a material volume of fluid can be expressed as:

$$\vec{M}(t) = \iiint_{\Omega} \rho \vec{v} d\Omega \tag{11}$$

where, $\vec{v}$ is the fluid velocity and Ω is the volume of the particle group. Note that the boundary of the particle group or material volume is flexible. Using the transport theorem, the derivative of Eq (11) with respect to time is written as:

$$\frac{d\vec{M}}{dt} = \rho \iiint_{\Omega} \frac{\partial \vec{v}}{\partial t} d\Omega + \rho \iint_{s} \vec{v} u_n ds \tag{12}$$

where, u_n is the normal component of the velocity of the material volume surface. The positive normal direction is out of the material volume. Now we consider the Euler's equation for inviscid fluid:

$$\frac{\partial \vec{v}}{\partial t} + \vec{v} \nabla \vec{v} = -\nabla \left(\frac{p}{\rho} + gz \right) \tag{13}$$

Integrating both sides of the Euler's equation over the material volume yields:

$$\iiint_{\Omega} \frac{\partial \vec{v}}{\partial t} d\Omega + \iiint_{\Omega} \vec{v} \cdot \nabla \vec{v} d\Omega = \iiint_{\Omega} -\nabla \left(\frac{p}{\rho} + gz \right) d\Omega \tag{14}$$

By applying Gauss–Ostrogradsky theorem, the third order integral in Eq (14) is then written as

$$\iiint_{\Omega} \vec{v} \nabla \vec{v} d\Omega = \iint_{s} \vec{v} (\vec{v} \vec{n}) ds \tag{15}$$

and the RHS of Eq (14) can be written as

$$\iiint_{\Omega} -\nabla\left(\frac{p}{\rho}+gz\right)d\Omega = \iint_{s} -\left(\frac{p}{\rho}+gz\right)\vec{n}ds \tag{16}$$

Now Eq (14) can be rewritten as

$$\iiint_{\Omega} \frac{\partial\vec{v}}{\partial t}d\Omega = \iint_{s}\left[-\left(\frac{p}{\rho}+gz\right)\vec{n}-\vec{v}v_n\right]ds \tag{17}$$

where, normal component $v_n = \vec{v}\vec{n}$. Substituting Eq (17) into the second term of the LHS of Eq (12) results in the following equation:

$$\frac{d\vec{M}}{dt} = -\rho\iint_{s}\left[\left(\frac{p}{\rho}+gz\right)\vec{n}+\vec{v}(v_n-u_n)\right]ds \tag{18}$$

Now consider the boundary conditions of the material volume in the presence of an impacting object. The surface of the material volume consists of the free surface s_f, the body surface s_b and the far field surface s_∞. For each boundary, the normal fluid velocity v_n is equal to normal velocity of the volume boundary u_n. At free surface, the vertical coordination and pressure are zero. At far field, the volume boundary is considered as static, and pressure is purely static pressure. In summary, the boundary conditions at those three surfaces listed are the following:

$$s_f : p = 0, \quad z = 0, \quad v_n = u_n$$
$$s_b : v_n = u_n$$
$$s_\infty : u_n = 0, \quad p = \rho gz$$

Substituting the boundary conditions into Eq (18), yields

$$\frac{d\vec{M}}{dt} = -\rho\iint_{s_b}\left(\frac{p}{\rho}+gz\right)\vec{n}ds - \rho\iint_{s_\infty}\vec{v}\vec{v}_n ds \tag{19}$$

The impact force on the body is the water pressure integral over the interface, can be expressed as

$$F_{impact} = \iint_{s_b} p\vec{n}ds \tag{20}$$

Rearranging Eq (19),

$$\begin{aligned}\iint_{s_b} p\vec{n}ds &= -\frac{dM}{dt} - \rho\iint_{s_b} gz\vec{n}ds - \rho\iint_{s_\infty} \vec{v}v_n ds \\ &= -\rho\frac{d}{dt}\iint_{s_b} \phi\vec{n}ds - \rho\iint_{s_\infty} \vec{v}v_n ds - \rho\iint_{s_b} gz\vec{n}ds\end{aligned} \tag{21}$$

where, $\frac{d\vec{M}}{dt} = \frac{d}{dt}\iint_{s_b} \phi\vec{n}ds$ is easily deduced from (11) by Gauss–Ostrogradsky theorem, and integral $\rho\iint_{s_\infty} \vec{v}v_n ds$ will die out because the quadratic velocity is very small at s_∞.

It is known that $\rho\iint_{s_b} \phi n_{33} ds = -vA_{33}$ from the definition of added-mass, where A_{33} is added-mass of direction normal to surface. Further, A_{33} is related to submerged volume by an added-mass coefficient which can be evaluated numerically by potential flow theory, and yet also can be expressed theoretically for some simple shapes. In addition, the last term is simplified by Gauss theorem as $\rho\iint_{s_b} gz\vec{n}ds = -\rho g\iiint_{\Omega} ds = -\rho g\Omega$, which is simply the buoyancy. Thus,

$$F_{impact} = \frac{dA_{33}v}{dt} + \rho g\Omega \tag{22}$$

Now consider the presence of wave, where, the free surface is not quiescent and not horizontal. The slope of the free surface is then expressed as

$$\beta = -\arctan\frac{\partial\eta}{\partial x} \approx \frac{Hk}{\pi} \tag{23}$$

Hence the impact forces are decomposed into two directional components, which are

$$\begin{cases} F_x = F_{impact}\sin\beta \\ F_y = F_{impact}\cos\beta \end{cases} \tag{24}$$

The pendulum system is considered as a single degree of freedom system and is expressed in terms of the angular motion. Impact loading is the exciting moment with respect to the hinge, so one can express the impact moment in terms of F_x and F_y.

$$M_{impact} = F_x L\cos\theta + F_y L\sin\theta \tag{25}$$

where, L is the length of the pendulum and θ is the instant angular displacement. Neglecting vertical relative velocity between the body and free surface, the impact velocity is now $v = \left(c - \dot{\theta} L\cos\theta\right)\sin\beta$. Considering $\frac{dA_{33}}{dt}$ is also associated with $\dot{\theta}$ and θ, it is certain that the impacting system is a highly nonlinear dynamic system.

2.2.2. Wagner's method

The approach in the previous subsection was based on von Karman's (1929) solution without considering free surface elevation. Wagner's method accounting for the local free surface elevation is believed to yield accurate estimates of peak impact pressure. In Wagner's method, the body is approximated as a flat plate in uniform flow and this allows one to obtain the velocity potential of the flow, by solving boundary value problems. Consequently, the local water surface elevation can be included and a new expression of the wetted area is obtained. The velocity potential and its derivative in vertical direction can be expressed as follows:

$$\phi = -V\sqrt{wc^2 - x^2}, \quad at\ x < wc \tag{26}$$

and

$$\begin{aligned} \frac{\partial\phi}{\partial z} &= \frac{\partial\phi}{\partial x} - V \\ &= \frac{V}{\sqrt{1 - wc^2 / x^2}} - V, \quad at\ x > wc \end{aligned} \tag{27}$$

where, V is the velocity of uniform flow, wc is one half of the wedge width, x and z are the horizontal and vertical coordinates.

Integrating Eq (27) over time yields a free surface elevation which is associated with submerged width wc. There is also a geometry relationship between wc and local surface elevation depending on the specific shape of the structure, and that allows one to solve for wc. As long as the expression of the wetted length wc is obtained, the fluid potential can be simply expressed with potential theory, i.e. equation (26) is the flow

potential below a flat plate. The hydrodynamic impact force is then calculated using Bernoulli's equation. For a circular cylinder, the wetted length is $\sqrt{2}$ times the wetted length without local elevation, while the peak slamming coefficient at the initial time of impact is found to double the slamming coefficient without local elevation. The slamming coefficient is defined as

$$C_s = \frac{F_s}{\frac{1}{2}\rho V^2 D} \tag{28}$$

where, F_s is the impact force per length of the cylinder and D is the diameter. This result is a little higher than the experimental results from Campbell & Weynberg (1980), and thus is considered as a reasonable and conservative estimation. Table 5 provides a focused comparison between von Karman's method and Wagner's method on water entry into an initially calm free surface. One thing that should be noted is that, the potential flow method without local elevation consideration will lead to the results of von Karman's momentum conservation method, so the potential flow method without local elevation is generally also called von Karman's solution.

Generally, von Karman's method is less accurate than Wagner's method in estimating of peak pressure, but there are exceptions, because the 3-dimensional effects tend to reduce the impact loads by Faltinsen (2004). On the other hand, von Karman's method agrees well with the experimental values except as noted for the initial peak value. Moreover, in the wave impact problem, the free surface elevation will be expressed by various wave theories and the water entry doesn't have to be solved in the vertical direction. In this case, the local elevation estimation in Wagner's theory can be questionable, because the main contribution to the local free surface elevation will be the proceeding wave but not the actual impact which disturbs the flow. For dynamic problems with incoming waves, the momentum conservation method is far more robust than using potential theory, because the expression of potential for complex flow field may require a lot of computation using computational fluid dynamics. In fact, Wagner's theory is popular with the studies using Boundary Element Method. In this research

investigation, the theoretical model and computational model will be developed based on von Karman's theory.

2.2.3. Other physical consideration

It is not difficult to understand that the theoretical impact force reaches the maximum value or a very large value instantaneously, i.e. t=0. This is not physically precise, because the force cannot reach a large value instantly due to the compressibility of water. The compressibility gives the water a pressure upper limit that the water pressure may reach at most, which is

$$p_{\max} = \rho c_e V \tag{29}$$

where, c_e is the velocity of sound in the water, V is the flow velocity. It is noted that c_e will change dramatically if air bubbles present. When the water is subject to a disturbance, the disturbance will propagate in the fluid with the sound velocity. Obviously, the time duration leading to the maximum impact force is very short. Sarpkaya (1978) developed a model of rise time, assuming that the slamming coefficient increases linearly during the rise time. Sarpkaya also developed the global dynamic response transfer function of rigid cylinders, and found the transfer function is very sensitive to the duration of rise time assumed. When the rise time is larger than 1/100 sec, the transfer function dramatically loses its harmonic shape.

Air trapping may occur during the slamming, especially in the context of ship bottom slamming and wave breaking. In bottom slamming, the deadrise angles are small, so the water tends to trap air and form an air cushion. When the deadrise angle is 0, the peak impact pressure is proportional to impact velocity (Chuang 1967), rather than to square of the impact velocity as reflected in either von Karman or Wagner's theory. Increasing the deadrise angle will reduce the effect of air trapping.

.

Table 5. Comparison between von Karman's method and Wagner's method

	Slamming coefficient	Pressure at measured peak pressure instant	Peak pressure position
Wagner	High estimation	Good	Good
Von Karman	Low estimation	Good	Bad

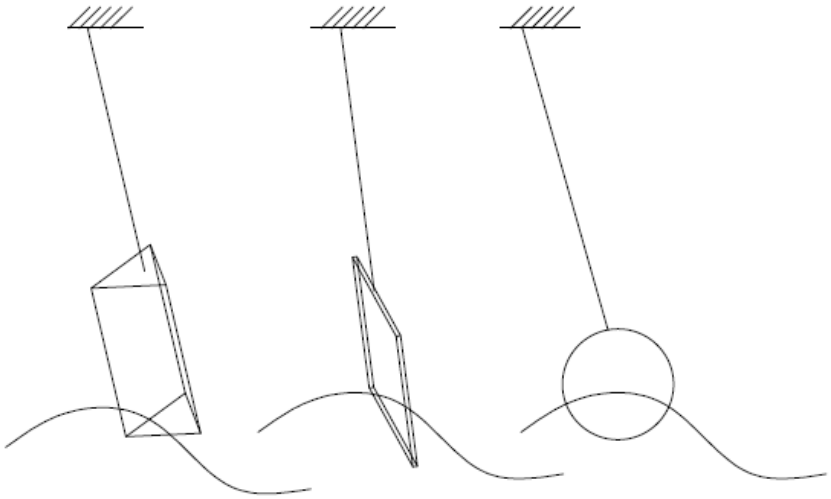

Figure 5. Pendulum bodies of different shapes

2.2.4. Wave impact of a spherical body

In this case, a pendulum with a spherical body is released above a progressive wave and impacts the wave (Figure 5). Weights can be added along the pendulum arm to change the natural period of the pendulum system. The length of pendulum, the height of the frictionless pivot and the radius of the sphere are known.

Viscosity is neglected and the damping force is not included in the following dynamic equations.

$$\left(m + m_{added}\right) l^2 \ddot{\theta} + mgl \sin\theta = M_{total} \tag{30}$$

$$M_{total} = M_{F-K} + M_{added\ mass} + M_{hydrostatic} \tag{31}$$

In order to calculate the total impact moment on the pendulum, the dynamic process of wave impact by the body is divided into four stages: fully submerged, mostly submerged, slightly submerged and not submerged, as illustrated in the Figure 6.

In the first stage, the whole sphere is submerged under the wave surface. The criterion of this stage is physically described as $h_u < \eta_u$, where, h_u and η_u are the vertical position and local wave elevation of the highest point on the sphere. The added-mass coefficient and Froude-Krylov force are present in this stage. The added-mass coefficient of a sphere is 0.5, according to classical analytical method, and Froude-Krylov force is given by Chakrabarti (1987):

$$\begin{aligned} F_x &= C_H \rho V \dot{u} \\ F_y &= C_V \rho V \dot{v} \end{aligned} \tag{32}$$

where, the velocities and accelerations are of the water particle located at the center of the sphere, and V is volume of the sphere. C_H and C_V are given coefficients. The Froude-Krylov force is induced from dynamic pressure under the wave, so the hydrostatic buoyancy which presents on a submerged body is not included. So, buoyancy must be calculated using Archimedes' principle and included in the inertia force. The fluid particle acceleration induced added-mass force is added to the Froude-Krylov force to form an integral inertia force. This contribution to the added-mass force is given by:

$$f_a = C_a \rho V \tag{33}$$

The other contribution of added-mass force due to response acceleration has been moved to LHS of the dynamic equation, see Eq (30).

The second stage of the wave impact modeling addresses when the water line is above the center of the sphere but is still lower than the top of the sphere, i.e. $h_u > \eta, h_{center} > \eta$. The components of the forces in this stage are the same as the fully submerged stage, but here the challenge is to calculate the instantaneous submerged volume. A computer program was developed to calculate the volume of the partly submerged sphere based on the strip method. By inputting the maximum submerged depth and the radius of the sphere, the submerged volume can be calculated. The maximum submerged depth is given by:

$$D_{ims} = (\eta - h_{center}) \cos a + R \tag{34}$$

where, $\alpha = -\arctan \frac{\partial \eta}{\partial x}$.

External forces in this stage are also the added-mass and Froude-Krylov force. The added-mass coefficients and Froude-Krylov force formula are approximated, based on an ideal hemisphere shape. Added-mass coefficients are still approximated by sphere added-mass coefficients. The Froude-Krylov forces are calculated by Chakrabarti's formula (1987) written as follows:

$$F_X = C_H \rho V[\dot{u} + C_3 \omega v] \tag{35}$$

$$F_Y = C_V \rho V[\dot{v} + C_4 \omega u] \tag{36}$$

where, C_H, C_V, C_3 and C_4 are coefficients from experiments. The volume V in (35), (36) and (33) becomes the submerged volume, because initial forces are due to fluid acceleration. Buoyancy that acts upward is also included.

The slightly submerged stage of the wave impact model is defined as the condition $h_{center} < \eta$, but the sphere is not totally outside the water. When the wave is high, the wave profile may be so steep that the body may be partially submerged in the wave profile even though the bottom of the body is not submerged at all. Hence, it is

difficult to identify the slightly submerged stage and not submerged stage. In this study, the whole wave surface within the projection of the sphere is examined. The range of the projected area is $\left[x-r, x+r\sin\theta\right]$. If any x_i that satisfies $\eta(x_i) > h(x_i)$ exists, the sphere is slightly submerged, otherwise it is not submerged. The variable $h(x_i)$ is given by

$$h(x_i) = h(x_0) - \sqrt{r^2 - (r-\Delta x)^2} \tag{37}$$

where, $x_0 = l\cos\theta - r$. In the slightly submerged stage, the submerged volume is calculated by integrating the discrete slice area over the submerged depth.

In the not submerged stage of the wave impact model, all external forces are equal to zero. For the slightly submerged stage, the forces consist of the inertia force and the impact force, due to the change of momentum of added-mass. The inertia force is obtained from the submerged volume and particle acceleration at an associated position. This stage utilizes Equations (35), (36) and (33) to calculate the inertia force, which is based on hemisphere, since the submerged volume is close to a hemisphere. The impact force is calculated from the change of momentum in terms of added-mass, as follows:

$$\begin{aligned}\frac{d(m_{added}v)}{dt} &= m_{added}\frac{dv}{dt} + v\frac{dm_{added}}{dt} \\ &= added\ mass\ force + v\frac{dm_{added}}{dt}\end{aligned} \tag{38}$$

where,

$$\frac{dm_{added}}{dt} = C_a\rho g\frac{dV_{added}}{dt} \tag{39}$$

and

$$\frac{dV_{added}}{dt} = \frac{\partial V_{added}}{\partial D}\frac{dD}{dt} + \frac{\partial V_{added}}{\partial \alpha}\frac{d\alpha}{dt} \tag{40}$$

where, D is immersed depth of radial direction and α is the inclined angle of the water line.

To simplify the differential equations, we assume α is a constant during the impact moment. So

$$\frac{dV_{added}}{dt} = \frac{V_{added}(D+\Delta D) - V_{added}(D)}{\Delta t} \tag{41}$$

where,

$$\Delta D = -\frac{d\left(l\cos\theta\right)}{dt}\Delta t = \dot{\theta} l \sin\theta \Delta t \tag{42}$$

And the submerged depth D can be obtained from the following technique. In Figure 7 AllD is a vector whose elements are the values of distance from the wave profile to the bottom of the sphere. The submerged depth is obtained by multiplying the median component with $\cos\alpha$.

2.2.5. Wave impact on a vertical flat plate

This impact of a vertical flat plate differs from sphere impact model in that the volume of the object is assumed to be zero, since the thickness of the flat plate is neglected. Therefore, the Froude-Krylov force associated with volume is neglect, and in this case the drag force due to the shape dominates. The drag force, known as Kutta-Zhukhovsky lift force, may be calculated using potential flow theory, and is given by the following expression:

$$\mathrm{L} = \rho U \Gamma \tag{43}$$

where, $\Gamma = 2\pi AU$ is the vortex strength and A is the area. The direction of the lift is the same as flow velocity U.

The added-mass of the plate per unit width is given by Wagner as:

$$m_{added} = \rho \frac{\pi}{2} b^2 \tag{44}$$

where, b is one half of the submerged length. The impact force is given by:

$$\frac{dm_{added}}{dt} v = \rho \frac{\pi}{2} 2b \frac{db}{dt} v \tag{45}$$

where, $\frac{db}{dt}$ can be expressed in terms of wave elevation rising rate and response velocity, that is

$$\frac{db}{dt} = \frac{1}{2}\left(\frac{d\eta}{dt} + \left|v\cos\theta\right|\right) = \frac{1}{2}\left(\frac{d\eta}{dt} + \left|\dot{\theta}l\tan\theta\right|\right) \tag{46}$$

where, v is the vertical component of response velocity. When impact force occurs, $\frac{db}{dt}$ should always be positive.

2.2.6. Wave impact on a vertical triangular body

Vertical triangular body can be used to simulate ship bows subject to slamming. This is similar to flat plate slamming but it is subject to both buoyancy and Froude-Krylov forces. The added-mass coefficient obtained from experimental data is approximately 1.2. The Froude-Krylov force is calculated based upon the difference of the wave induced pressure on the two sides or faces incident on the incoming wave. The pressure on each side is calculated from the integration of wave induced pressure over the submerged area.

$$F_{f-k} = \iint_{s-left} p(x,z)dxdz\tan\frac{\theta}{2} - \iint_{s-right} p(x,z)dxdz \tag{47}$$

where, θ is the vertex angle of the cross-section, and p(x, z) is the pressure field of the 2-dimensional wave. For the left side of the cylinder, which is the upstream side, a double integral must be performed. To reduce the model computation, the integration over z-direction is obtained analytically, and the integration over x-direction is evaluated numerically using a trapezoidal scheme in the code. The analytical integral of pressure over z-direction is written as:

$$\int_{left} p(x,z)dz = \rho\frac{gH}{2}\frac{\sinh k(d+\eta) - \sinh k(d+e-b)}{\cosh k(d+\eta)}\cos(kx-\omega t) \tag{48}$$

where, d is water, $\eta = \eta(x)$ is local wave elevation, e is the coordinate of the center of gravity, and b is one half length of the cylinder. This result is then integrated over x.

The slamming force is calculated only when the wave impacts the sharp side of the triangular body. The submerged volume is calculated from:

$$V = (\eta_1 + h - d)S + (\eta_2 - \eta_1)S/3 \tag{49}$$

where, η_1 and η_2 are respectively the wave elevation of the flat and sharp sides, h is the y-coordination of the gravity center of the cylinder, d is the distance from the lower end to the gravity center, and S is the cross-section area. The volume is needed to evaluate the buoyancy force. The slamming force is equal to the increasing rate of added-mass:

$$F = \rho C_a \frac{dV}{dt} v = \rho C_a \tan\alpha S v^2 \tag{50}$$

where, v is the relative horizontal velocity between structure and wave, the slope $\alpha = (\eta_2 - \eta_1)/r$, and r is the height of the triangular cross-section.

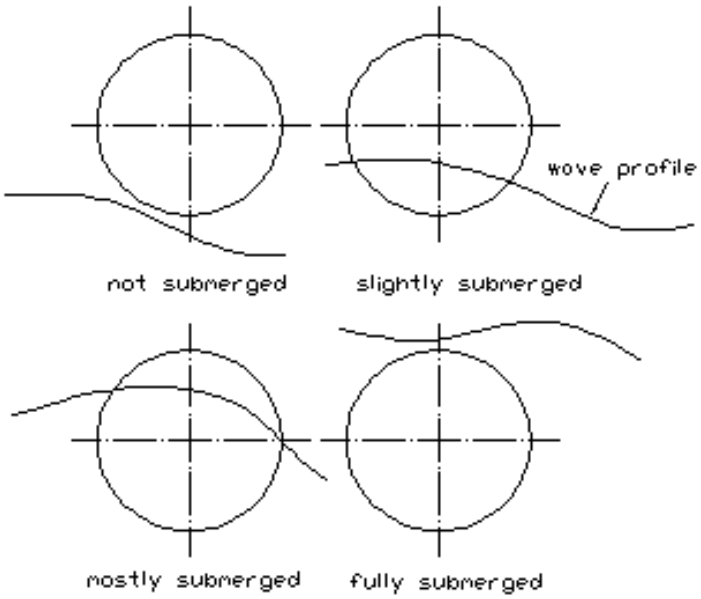

Figure 6. Four stages of sphere impact.

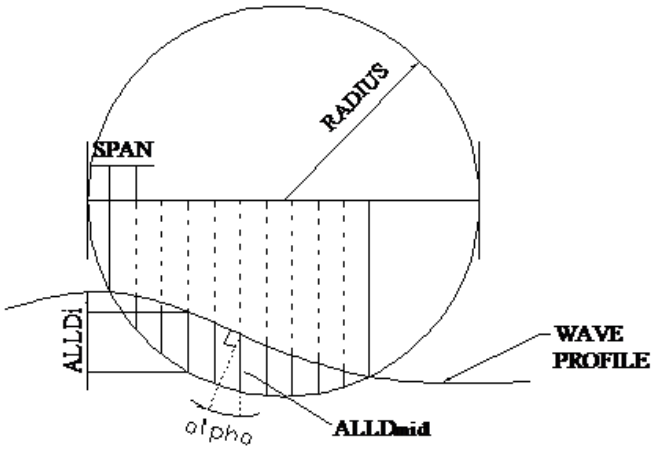

Figure 7. Illustration of the technique to calculate submerged depth

3. NUMERICAL ANALYSIS OF PENDULUM SYSTEMS

This section presents the numerical simulation results for the various body shapes impacting the face of a wave. The numerical models are based on the ordinary differential equations of motion for pendulum systems, with slamming loads estimated based upon von Karman's formula. All the wave loads are associated with the motion of the pendulum and updated over time. The results of numerical simulation are also compared with previously published experimental data and the classification society's rules. The effects of some hydrodynamic coefficients are discussed based on the numerical models.

3.1. Wave impact on a spherical body

Specific parameters for this numerical simulation are as following:

Length of pendulum: 2.0 m
Radius of sphere: 0.1 m
Mass of sphere: 10 kg
Height from water level to pivot: 2.0 m
Natural Frequency: 0.35 Hz
Initial impact velocity: 4.2 m/s
Wave height: 0.4 m
Wave period: 0.2 ~ 2 s (0.5 ~5 Hz)
Initial angle: 60°

The graphs presented in this subsection illustrate the dynamic response of the spherical body subjected to a range of wave conditions. Wave periods in the range of 0.2~2s represent a range of wave periods of 2~20s in the real world assuming a Froude scaling of 1:100. Due to nonlinearity, the response spectra are not always dominated by exciting frequency. For high wave frequency, neither the exciting frequency nor natural

frequency is observed in the response spectra, while the dominating response frequency is located between them (see Figures 8 and 9). For low wave frequencies, the exciting force input per unit time decreases, and thus the total exciting energy is reduced. The motion of the pendulum is not disturbed by the wave as much as it is in the case of high frequency excitation. Therefore, the natural frequency dominates the response spectra for low wave frequencies (see Figure 10 - Figure 15).

Consider the case where the pendulum arm is increased in length and the mass is increased to cause the spherical body always be submerged in the wave profile. In this situation the pendulum is not subject to wave impact forces, rather the body is subjected to only usual wave forces modeling using Morison's equation. It is interesting that the natural frequency and exciting frequency are clearly observed (See Figure 16). When the exciting frequency is close to the natural frequency, the subharmonic responses are clearly observed in Figure 17. Those properties are not observed in the spectra for the case of wave impact. This indicates that the impact force brings considerable nonlinearity to the system and makes the response spectra less predictable.

The total slamming force is composed of the inertia force, the impact force and the buoyancy force. Figures 18, 19 and 20 present the time series of these three slamming force components resulting from the impact of the spherical body with a wave whose frequency is a 1 Hz. Note that the three components as presented cannot simply be added together as their vectors may not be aligned. Among these three force components, the impact force usually dominates the total force, but that is not always the case, as the deadrise angle has a large influence on the importance of impact force.

The peak impact force can be studied using the pendulum without the wave field, i.e. using calm water in the tank. The relationship between the initial height of the spherical body above the free surface and the resulting impact force is presented in Figure 21.

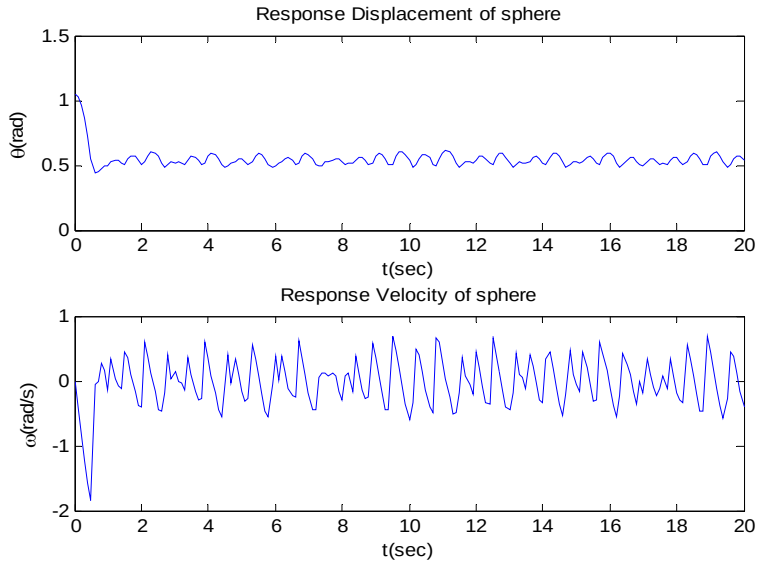

Figure 8. Time history of motion for sphere, wave frequency =5 Hz

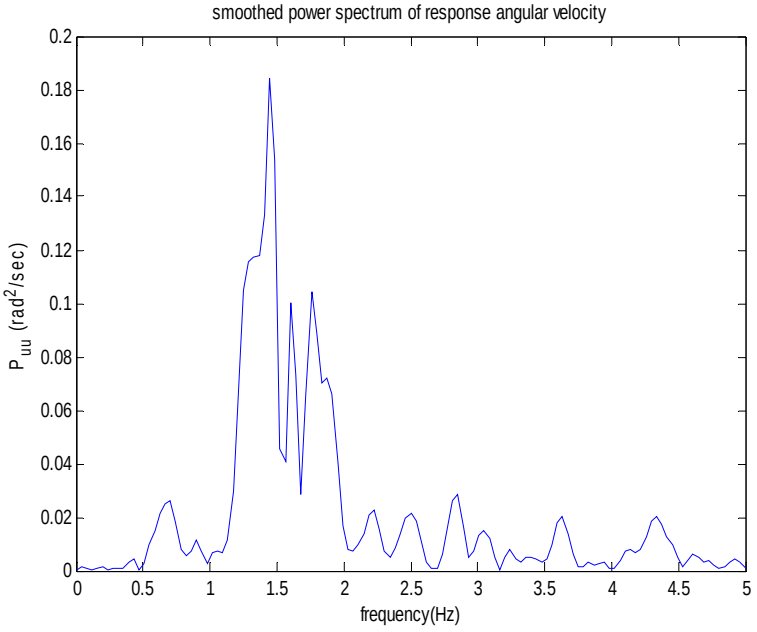

Figure 9. Response spectrum of velocity for sphere, wave frequency =5 Hz

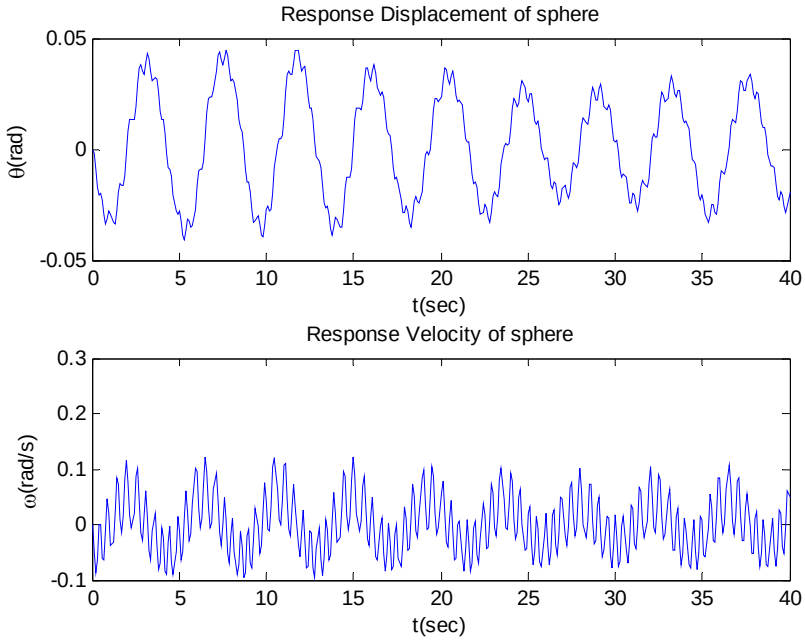

Figure 10. Time history of motion for sphere , Wave frequency=2 Hz

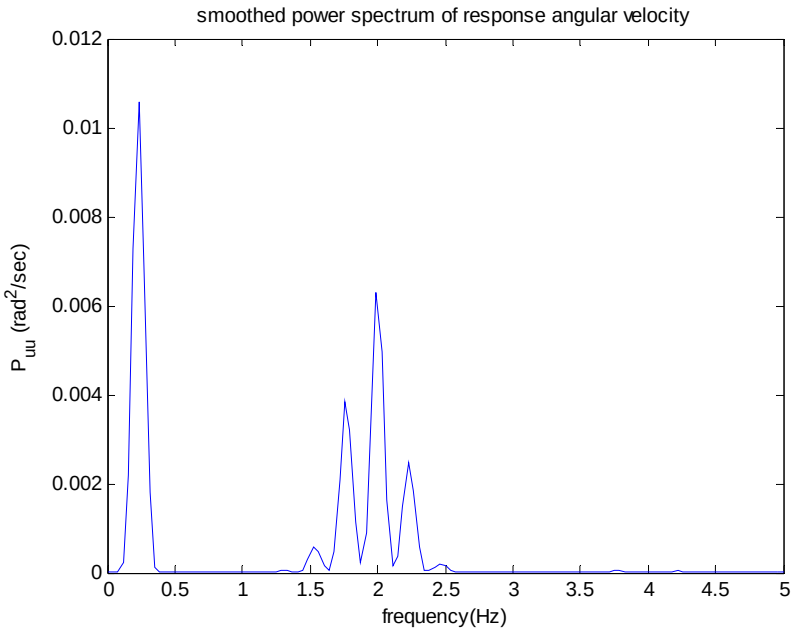

Figure 11. Response spectrum of velocity for sphere, wave frequency = 2 Hz

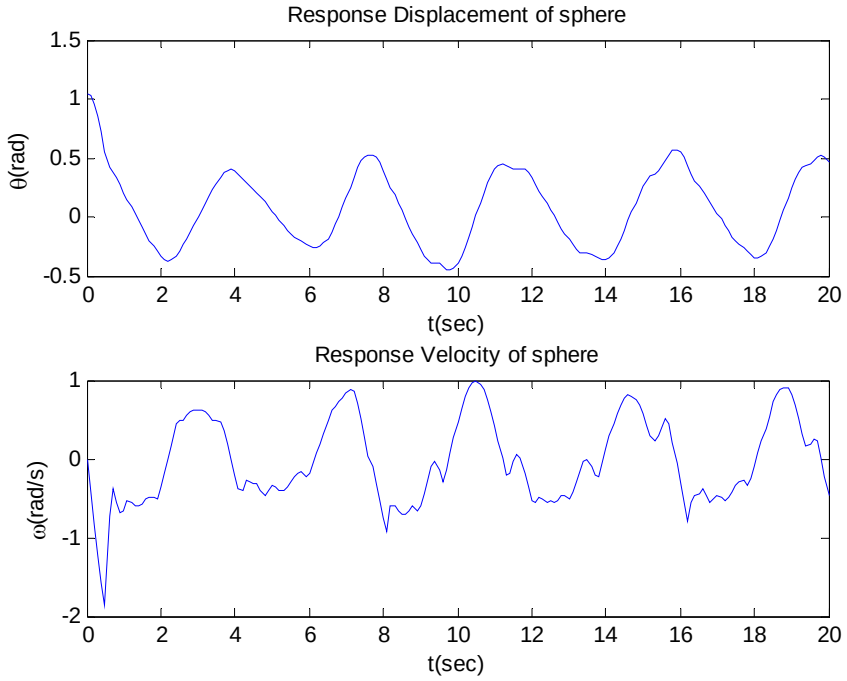

Figure 12. Time history of motion for sphere, wave frequency =1 Hz

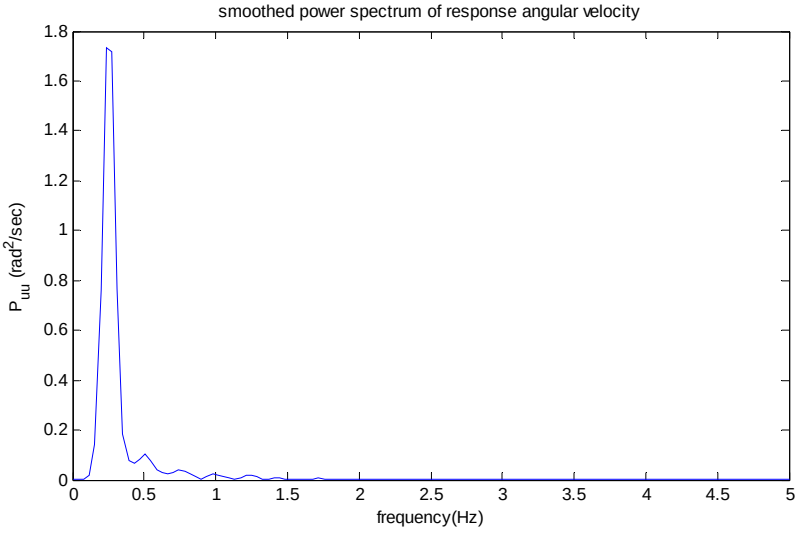

Figure 13. Response spectrum of velocity for sphere, wave frequency = 1 Hz

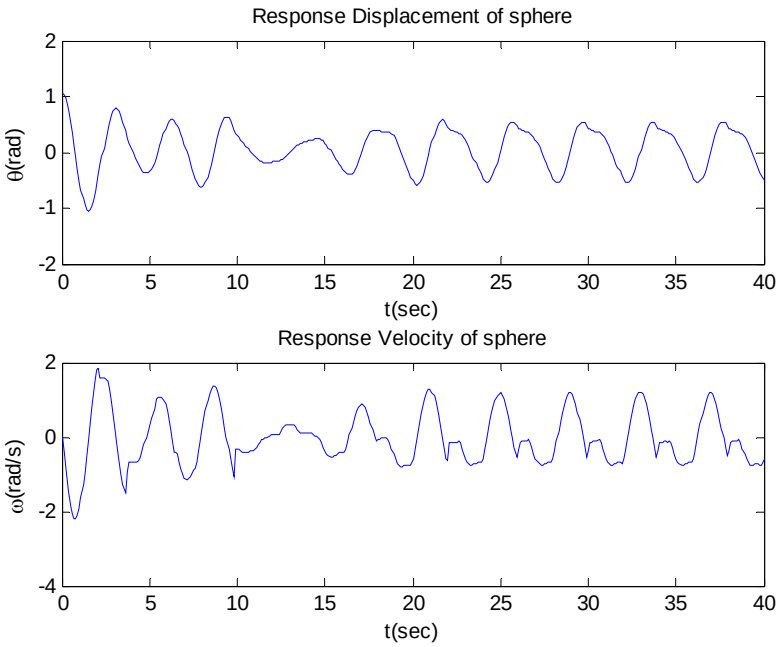

Figure 14. Time history of motion for sphere, wave frequency=0.5 Hz

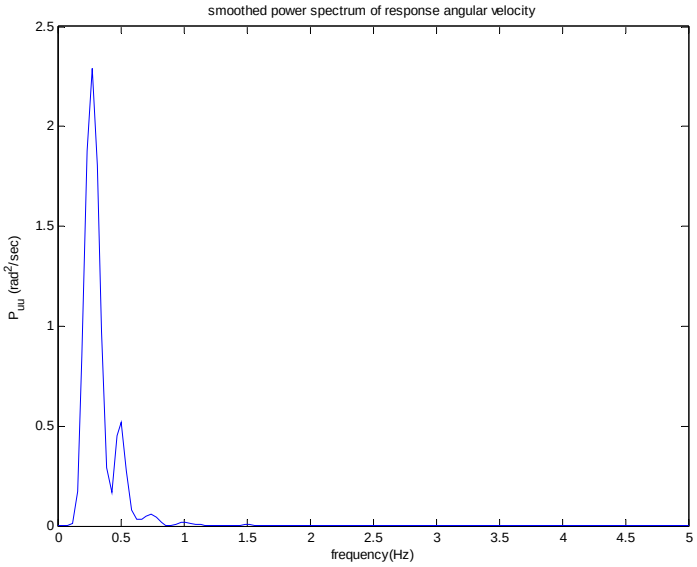

Figure 15. Response spectrum of velocity for sphere, wave frequency =0.5 Hz

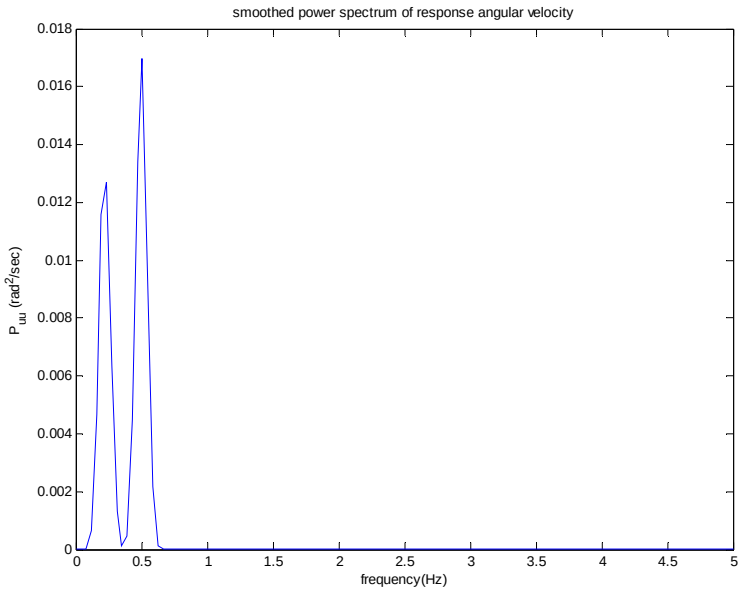

Figure 16. Without impact, nature frequency and exciting frequency for sphere

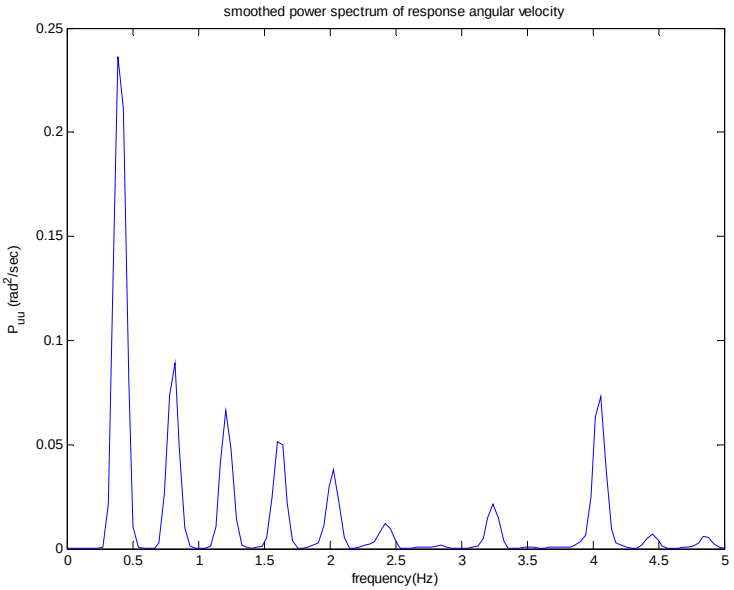

Figure 17. Subharmonic response for sphere

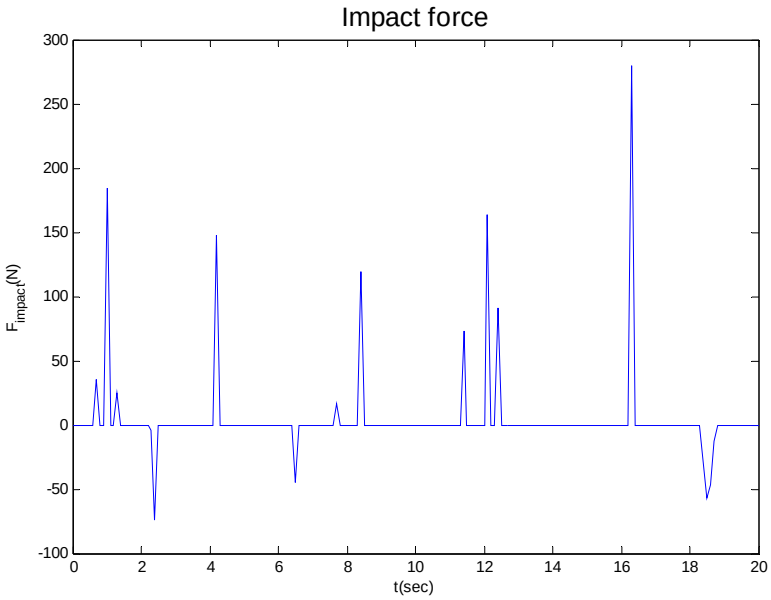

Figure 18. Impact force for sphere, wave frequency= 1 Hz

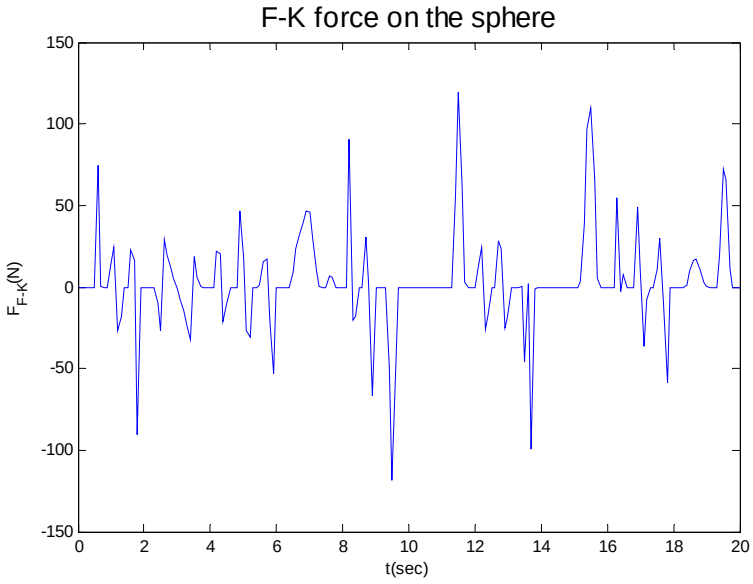

Figure 19. F-K force for sphere, wave frequency= 1 Hz

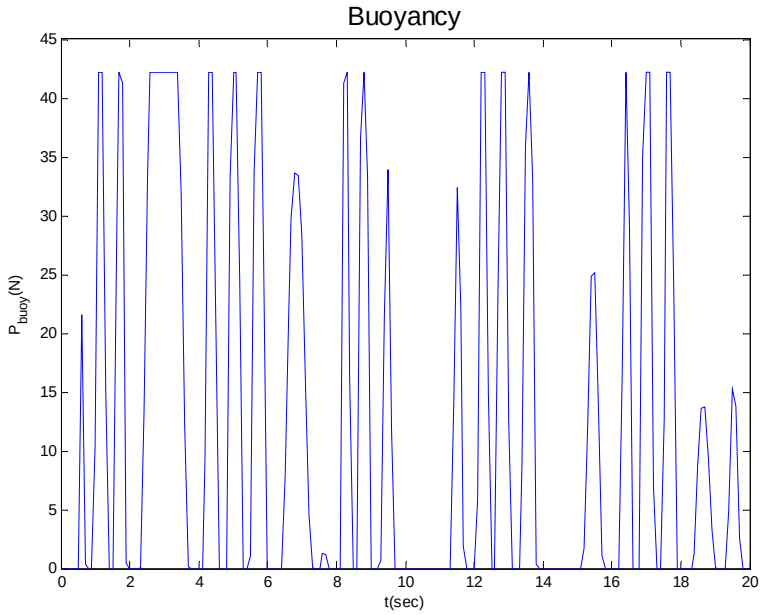

Figure 20. Buoyancy for sphere, wave frequency= 1 Hz

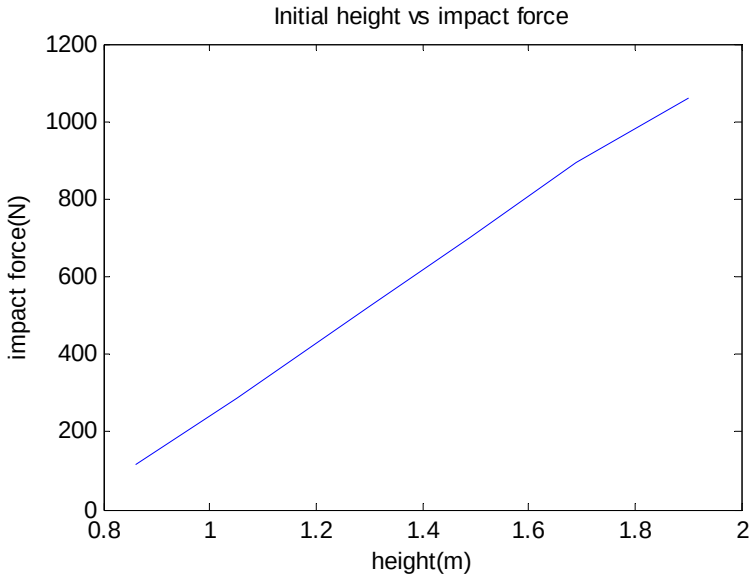

Figure 21. Initial height versus impact force for sphere, pivot height=2m, calm water

3.2. Wave impact on a vertical triangular body

Specific parameters for this numerical simulation of a vertical triangular body are as following:

Length of pendulum: 2.0 m
Cross-sectional triangle height: 0.1 m
Vertex angle: 45°
Distance from center of gravity to the end of cylinder: 0.3m
Mass of weight: 10 kg
Height from water level to pivot: 2.0 m
Natural Frequency: 0.35 Hz
Initial impact velocity: 4.2 m/s
Wave height: 0.2 m
Wave period: 0.5 ~ 3s (1/3~ 2 Hz)
Initial angle: 0°

The graphs in this subsection present the time series of response displacement and velocity of the triangular cross-sectional pendulum subjected to different wave frequencies. Using 1:100 Froude scaling, wave periods in the range of 0.5~3s represents wave periods in the range of 5~30s in ocean environments. Power spectra of response velocity are presented to illustrate the relationship between response and incoming wave in the frequency domain. (See Figure 22 – Figure 29).

Based upon the following power spectra for different exciting wave frequencies, it is found that the frequency of response purely consists of the wave frequency and the natural frequency which is close to 1/3 Hz. In the Figure 23, a subharmonic response is observed at 4 Hz that is double the exciting wave frequency. A typical resonant behavior is observed when the exciting frequency is 1/3 Hz. The magnitude of response is found to be in the range of 5~50 times larger than those not subjected to resonant excitation. The response of resonance becomes stable at some value, because of the damping, which

is mainly resulted from the drag force. When the wave is removed and the cylinder impacts on the calm water, the motion damps out as time progresses (see Figure 30).

Contrary to the spherical body, the forces of vertical triangular body impact model mostly result from free surface slope. Therefore, the force obtained from calm water impact has a very small impact force component. In the Figure 31 and Figure 32, comparing the magnitude of impact force with drag force, it is found that impact force does not dominate the total force, but the buoyancy and drag force do. The reason is that, for the vertical triangular body model, the body face is nearly perpendicular to the free surface, so the impact is not as strong as for the sphere, while on the sphere's surface, some part is always parallel to the free surface and the rate of increase in added-volume is very large. For the same reason, the slamming force of the vertical triangular body is not obviously affected by the impact angle. The buoyancy force is presented in the Figure 33.

Besides the impact angle, another factor affecting slamming loads is the shape of the body. For the vertical triangular body model, it is found that the waterline area largely affects the impact force. To change the waterline area, simply change the vertex angle from 45° to 60° and plot new results (see Figures 34 - 38). The results show that increasing the vertex angle or waterline area will increase the impact force. This conclusion is in accord with the extant knowledge in naval architecture that a slimmer bow reduces the wave impact and inertia force by piercing waves. Figure 38 illustrates the total slamming forces on the vertical triangular body.

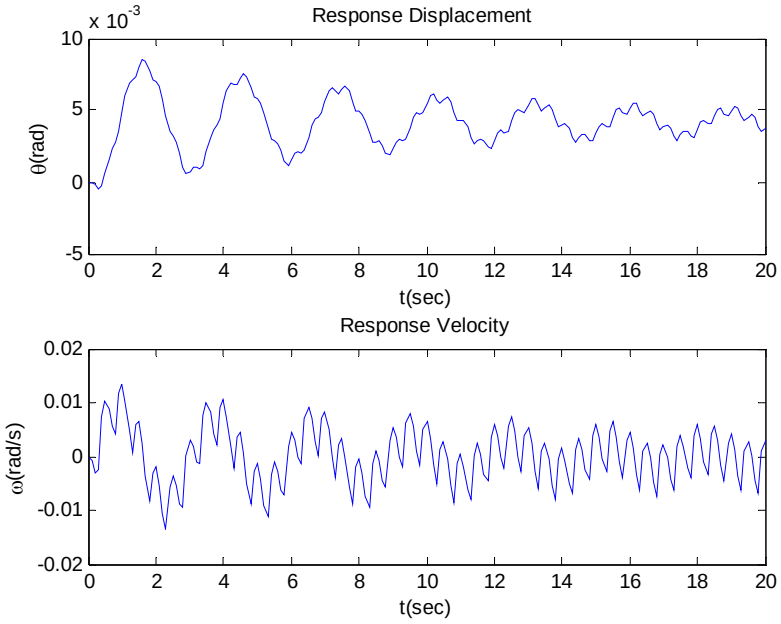

Figure 22. Time history of motion for vertical triangular body, wave frequency=2 Hz

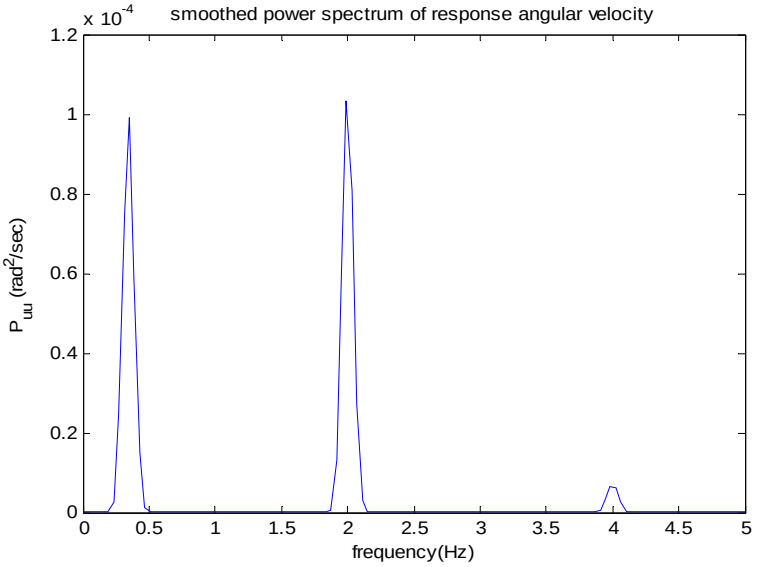

Figure 23. Response spectrum for vertical triangular body, wave frequency=2 Hz

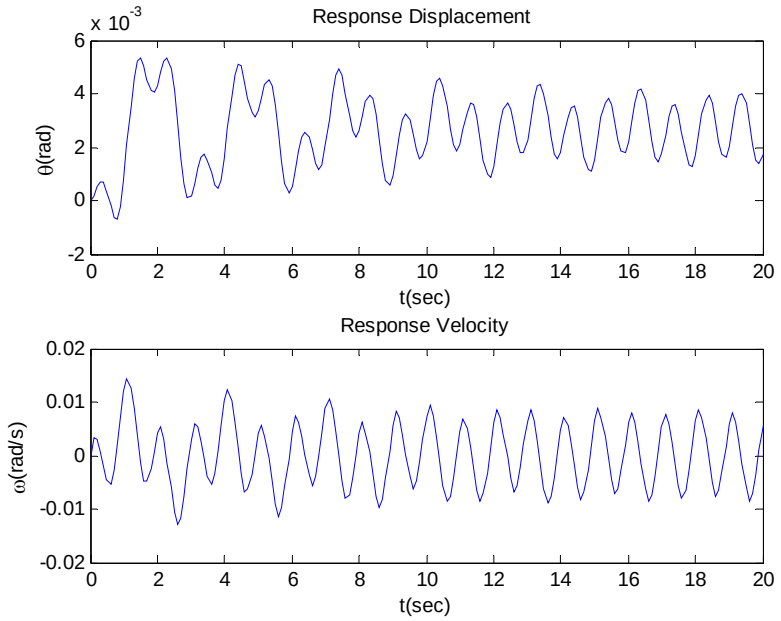

Figure 24. Time history of motion for vertical triangular body, wave frequency= 1 Hz

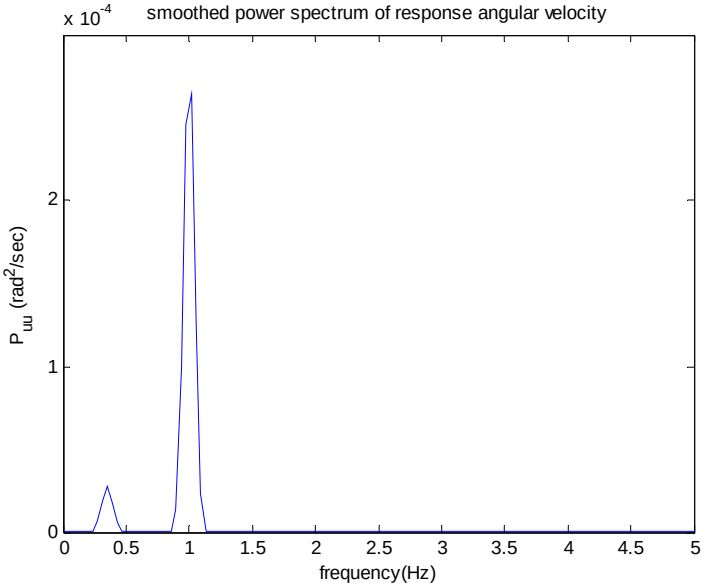

Figure 25. Response spectrum for vertical triangular body, wave frequency= 1 Hz

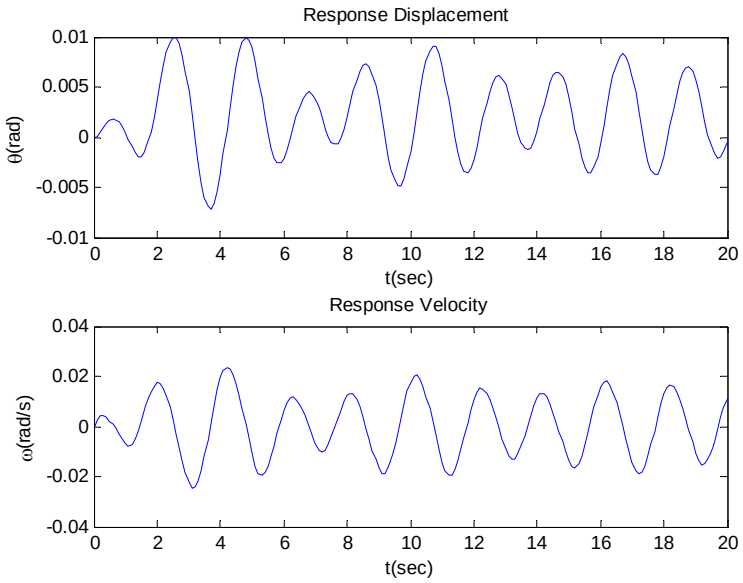

Figure 26. Time history of motion for vertical triangular body, wave frequency= 0.5 Hz

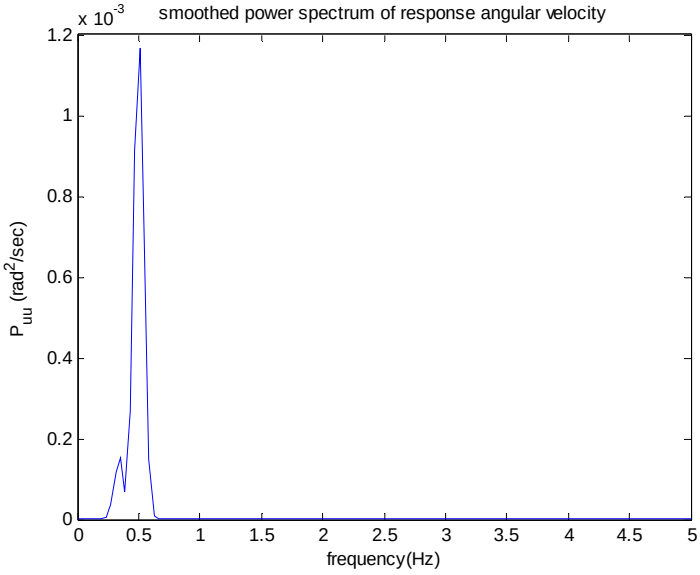

Figure 27. Response spectrum for vertical triangular body, wave frequency= 0.5 Hz

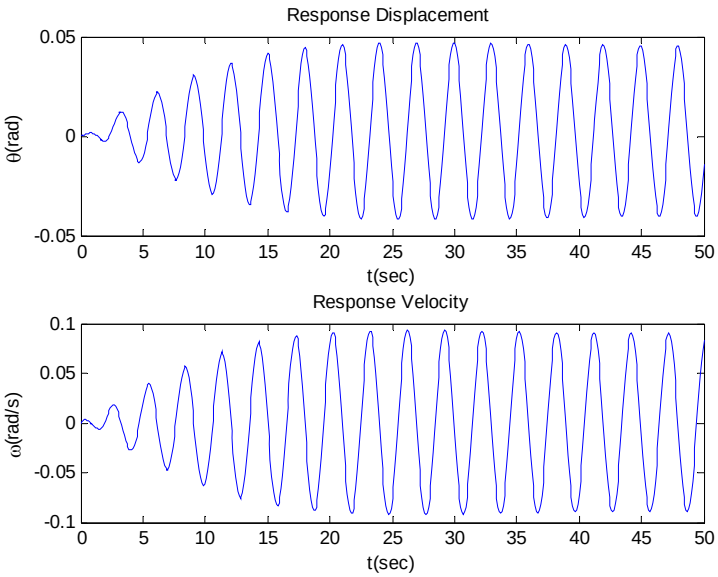

Figure 28. Time history of motion for vertical triangular body, wave frequency= 1/3 Hz

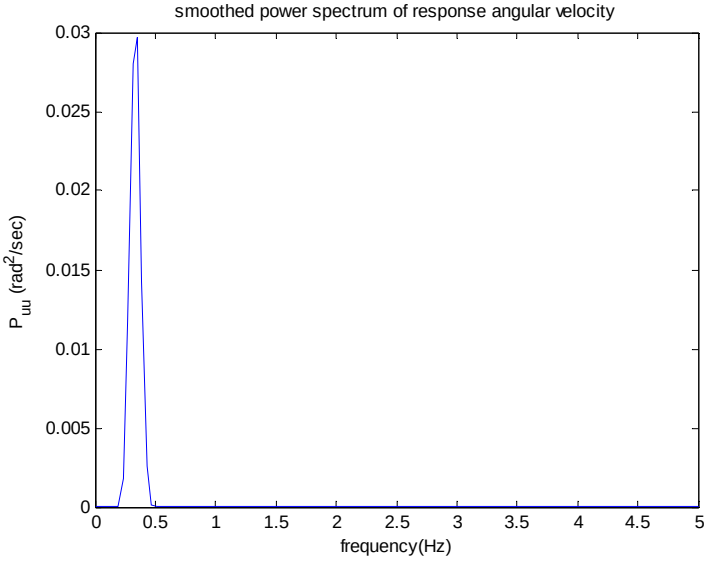

Figure 29. Response spectrum for vertical triangular body, wave frequency= 1/3 Hz

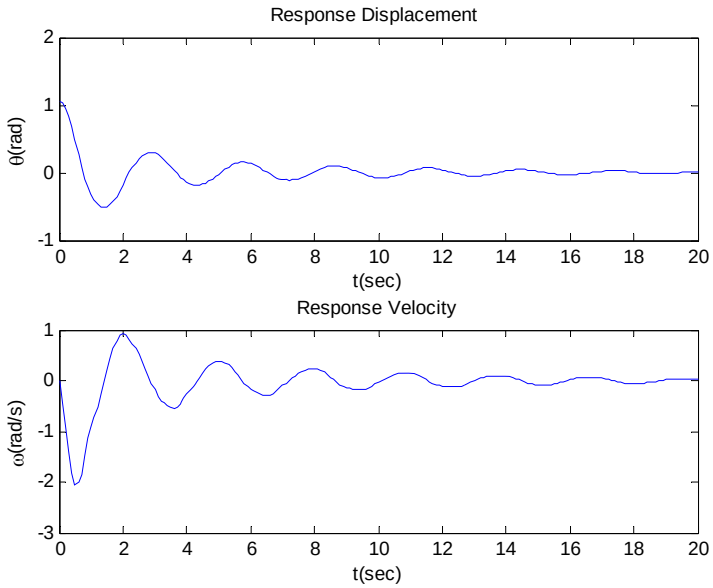

Figure 30. Time history of motion for vertical triangular body in calm water

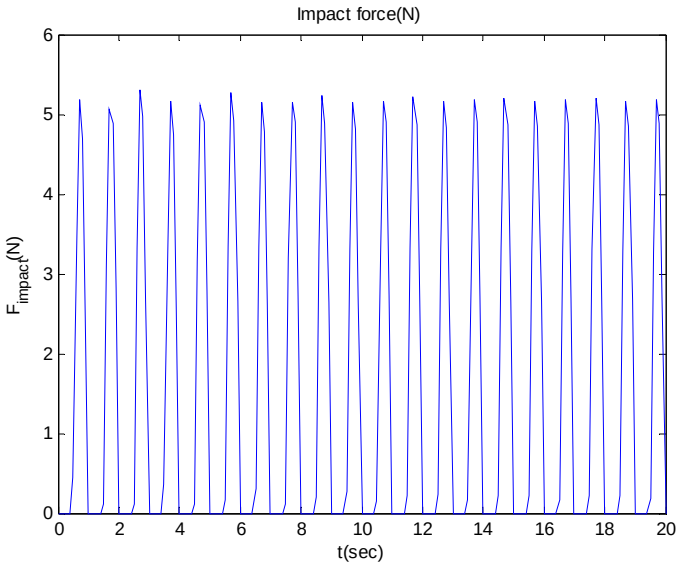

Figure 31. Impact force on vertical triangular body, wave frequency= 1 Hz

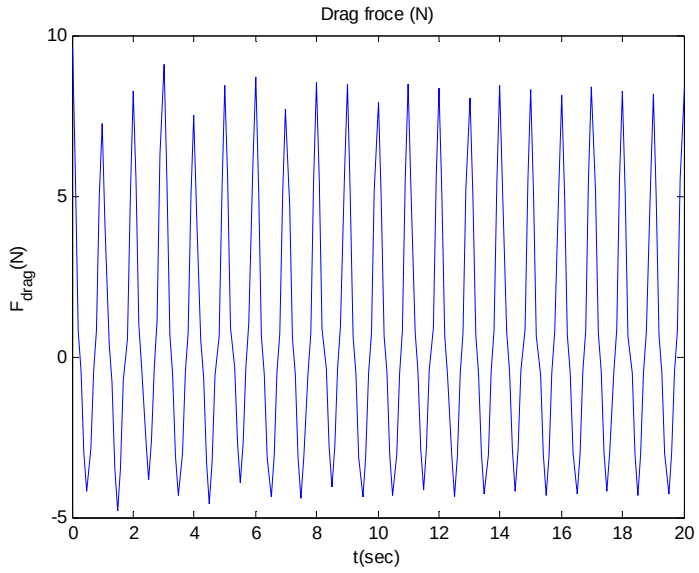

Figure 32. Drag force on vertical triangular body, wave frequency= 1 Hz

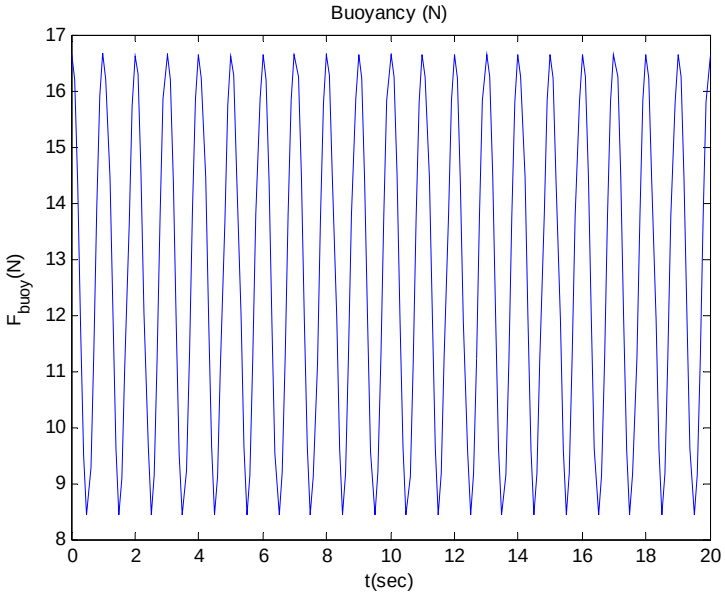

Figure 33. Buoyancy of vertical triangular body, wave frequency= 1 Hz

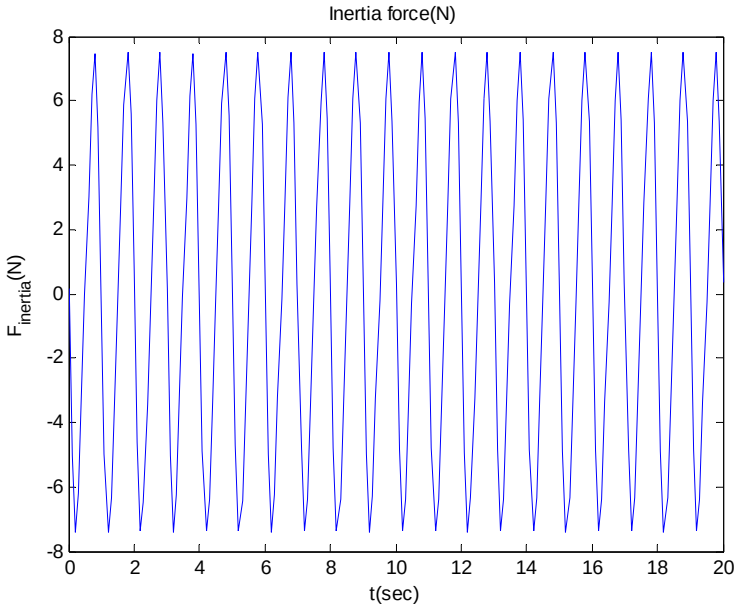

Figure 34. Inertia on vertical triangular body, wave frequency= 1 Hz

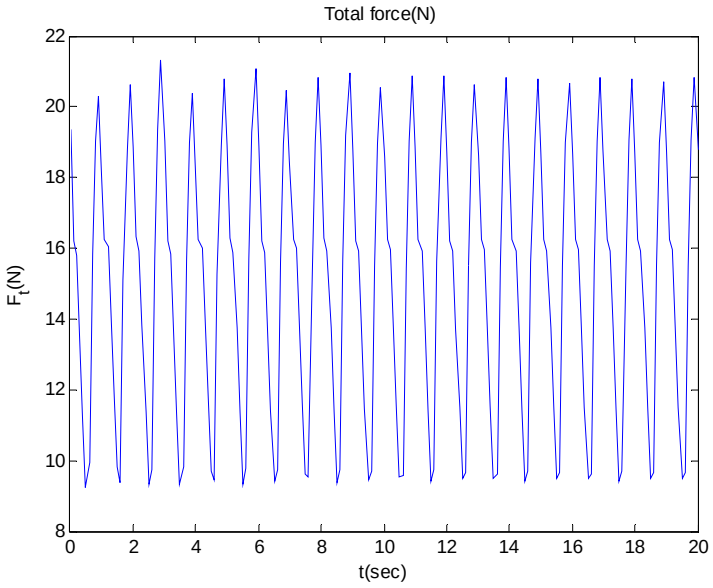

Figure 35. Total force on vertical triangular body, wave frequency= 1 Hz

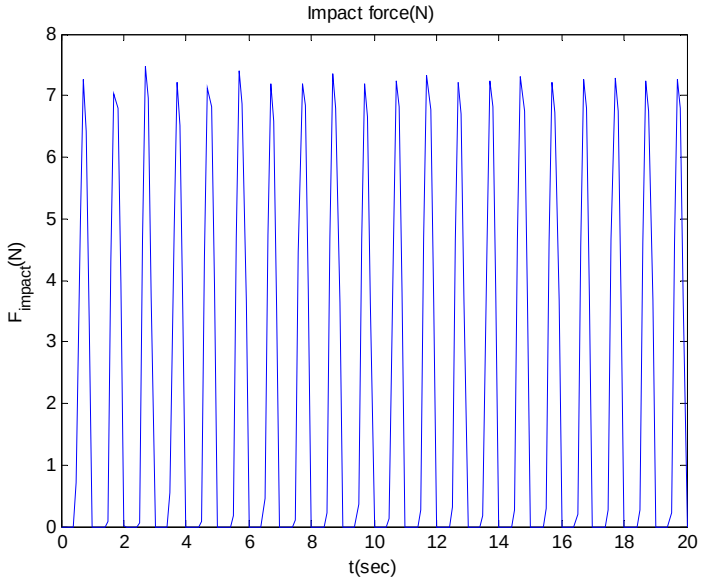

Figure 36. Impact on vertical triangular body(vertex angle 60°), wave frequency= 1 Hz

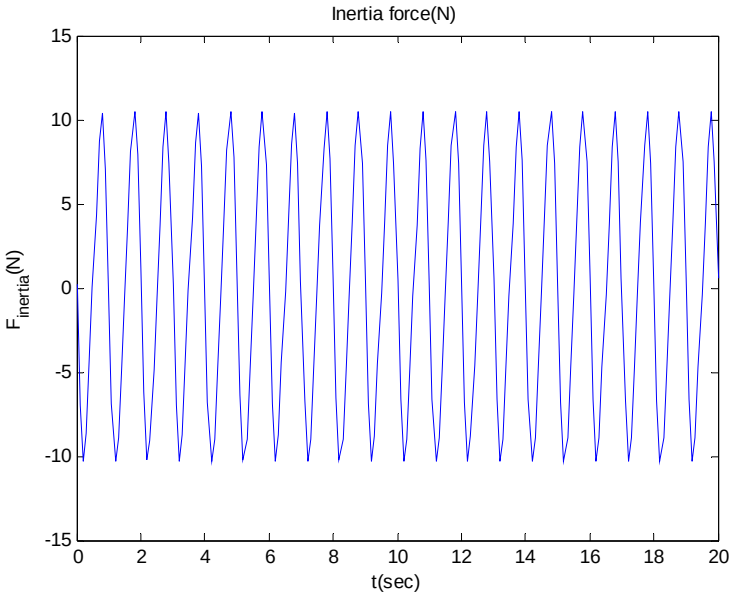

Figure 37. Inertia force on vertical triangular body (vertex angle 60°), wave frequency= 1 Hz

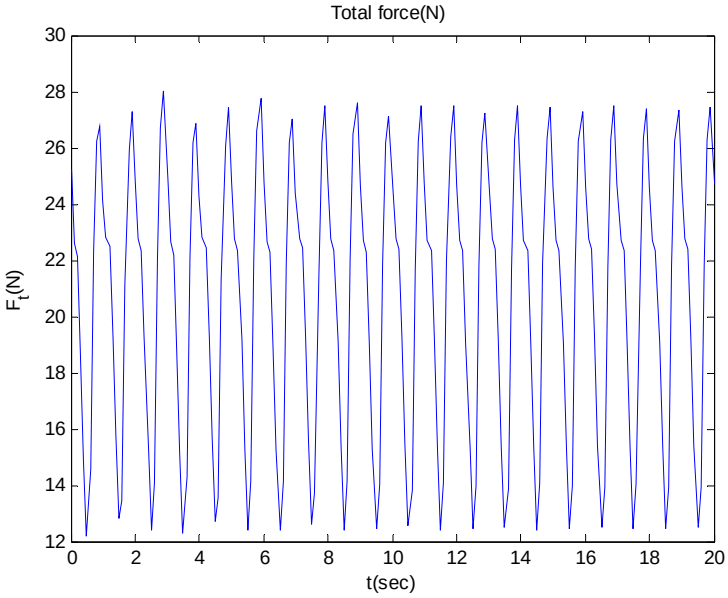

Figure 38. Total force on vertical triangular body (vertex angle $60°$), wave frequency= 1 Hz

3.3. Wave impact on a vertical flat plate

In this case, the inertia force is comprised of Froude-Krylov force and added-mass force, which are both related to the volume. The drag force is associated with the length scale in the flow direction. Since the thickness of the plate is neglected, the system will not experience inertia force and drag force, but it is subject to lift force and the plane body is still massive. Specific parameters for this numerical simulation are as following:

Length of pendulum (from pivot to the center of gravity): 2.0 m
Half width of the plate (from the center of gravity to the lower edge): 0.1 m
Mass of weight: 20 kg
Height from water level to pivot: 1.9 m
Natural Frequency: 0.35 Hz
Wave height: 0.2 m
Wave period: 0.5 ~ 3s
Initial angle: 5.7°

The graphs in this subsection illustrate the dynamics response of the flat plate. Based upon 1:100 Froude scaling, the wave periods in the range of 0.5~3s reflects the wave periods of 5~30s in ocean environments. Power spectra of response velocity are presented to explore the relationship between response and incoming wave in the frequency domain. The natural frequency 0.35 Hz represents a compliant system with a natural frequency of 0.035Hz. Based upon the time history of displacement in the Figure 39, 41 and 43, the flat plate is found to oscillate about a positive angle, while Figure 45 shows the oscillation excited by a low exciting frequency is about the equilibrium position of the pendulum, because for low exciting frequency, the pendulum has enough time to restore its original position between two impacts.

In the power spectra, it is observed that the frequencies of response are strongly related to incoming wave frequency, especially for the situations with low exciting

frequencies. The natural frequencies of the pendulum are not obvious in the power spectra, because the plate impact system has very large damping due to the lift force. For a 2 Hz wave frequency, the peak response is found between 2 Hz and 1 Hz where there is neither the exciting frequency nor the natural frequency, and some response frequencies are also found lower than 1 Hz, which is related to natural frequency. In fact, several subharmonic response frequencies are observed (see Figure 40). For 1 Hz, 0.5 Hz and 1/3 Hz wave frequency, the peak response frequencies are all found at the exciting frequencies (see Figure 42, 44 and 46). For 1/3 Hz wave, the exciting frequency is very close to the natural frequency of the pendulum, but no resonant response is observed because of the strong damping. Compared to spherical body impact and vertical triangular body impact, the pendulum natural frequency is not presented in the response spectra, because the natural frequency is always changed by large damping which varies over time. For low exciting frequency, the response time history displays more harmonic than high frequency, where groups are found in the response time series.

The forces acting on the plate impact model differ from those acting on the sphere and vertical triangular body models. Since no volume is considered for the plate, there is no Froude-Krylov force. The damping force will be a lift force raised from potential flow theory, rather than viscous drag force, because the thickness is neglected. In the Figure 47 and Figure 48, comparing the magnitude of impact force with lift force, it is found that the magnitude of impact force and lift force are similar. This is because the body face is nearly perpendicular to the free surface, which is similar to the vertical triangular body model. For the plate impact model, the impact on the plate is not affected by the impact angle, and there is no shape parameter of a plate affecting impact like the waterline area of the vertical triangular body model.

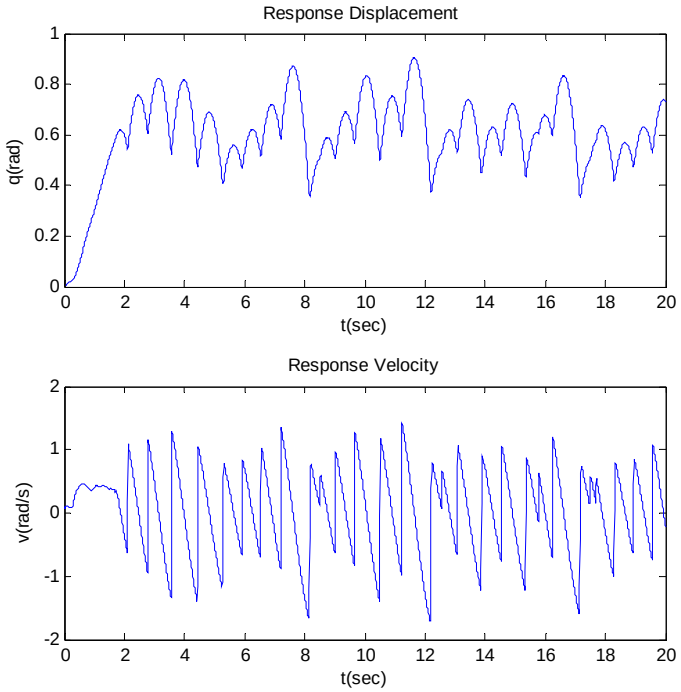

Figure 39. Time history of motion for flat plate, wave frequency =2 Hz

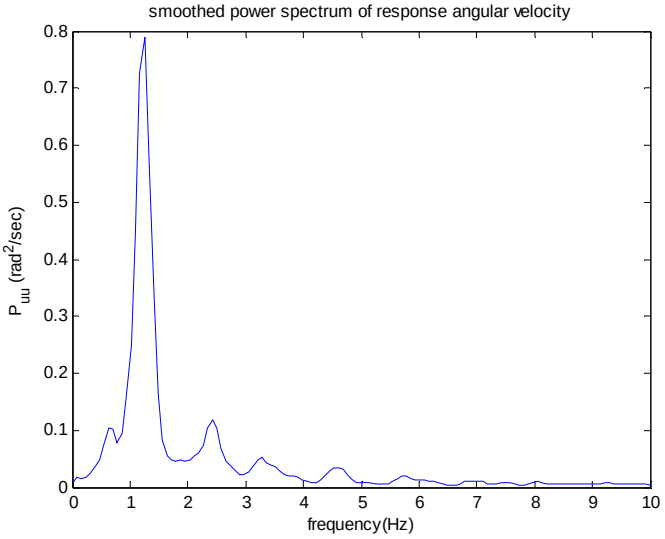

Figure 40. Power spectrum for flat plate: wave frequency =2Hz

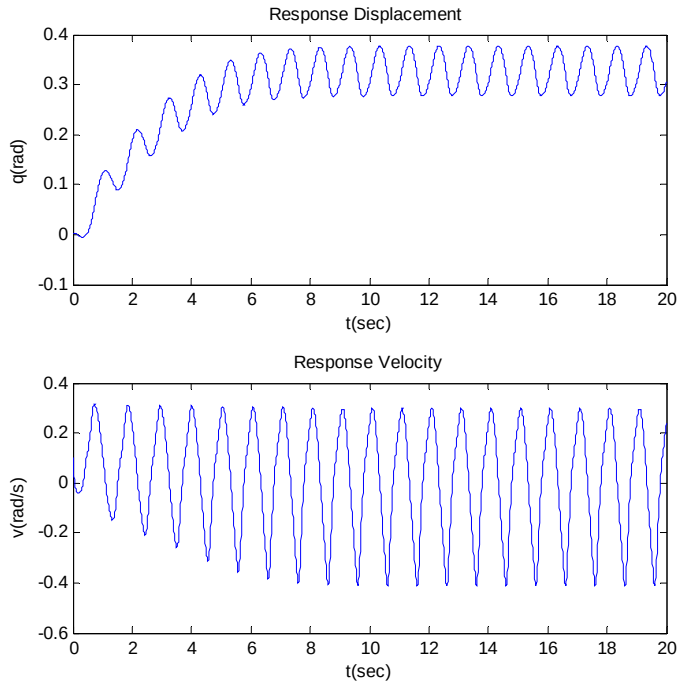

Figure 41. Time history of motion for flat plate, wave frequency=1 Hz

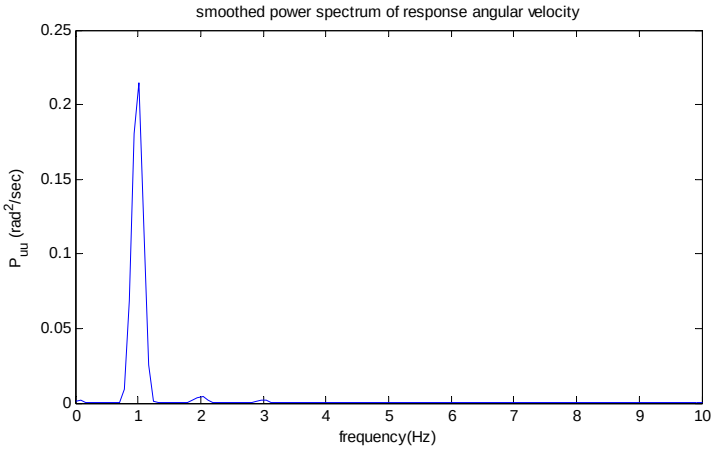

Figure 42. Power spectrum for flat plate: wave frequency =1Hz

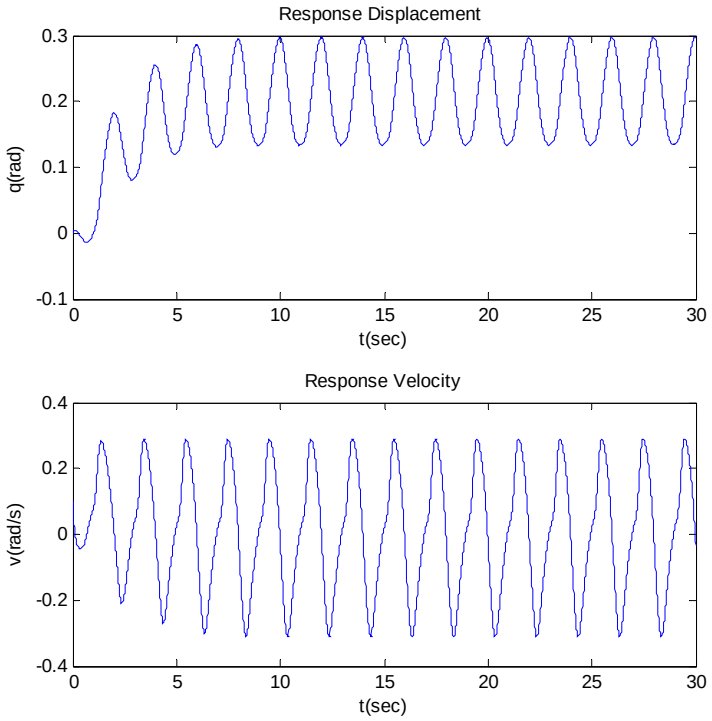

Figure 43. Time history of motion for flat plate, wave frequency= 0.5 Hz

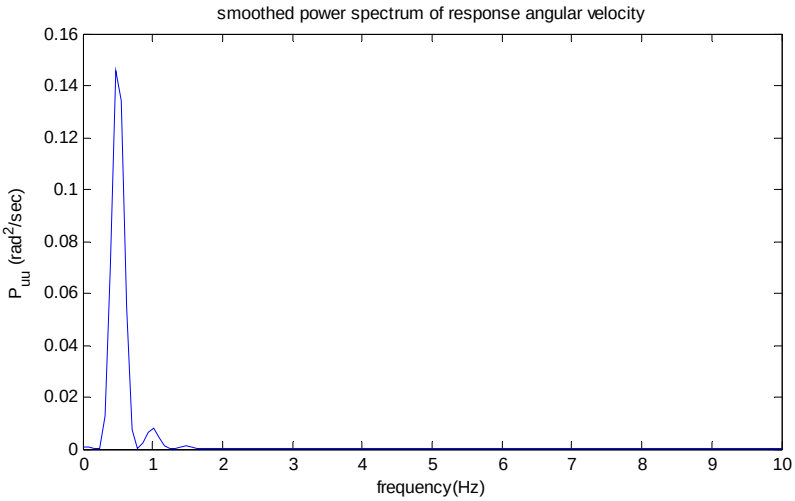

Figure 44. Power spectrum for flat plate: wave frequency =0.5 Hz

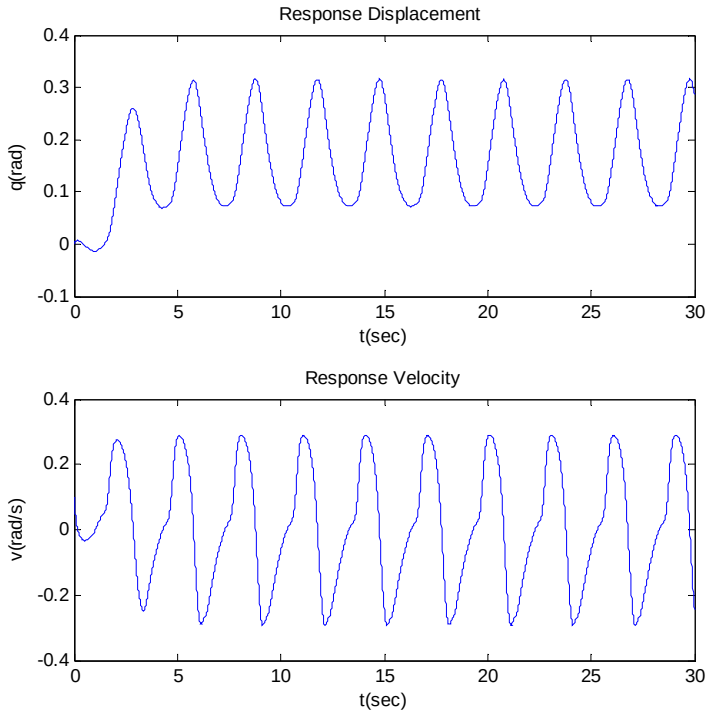

Figure 45. Time history of motion for flat plate, wave frequency= 1/3 Hz

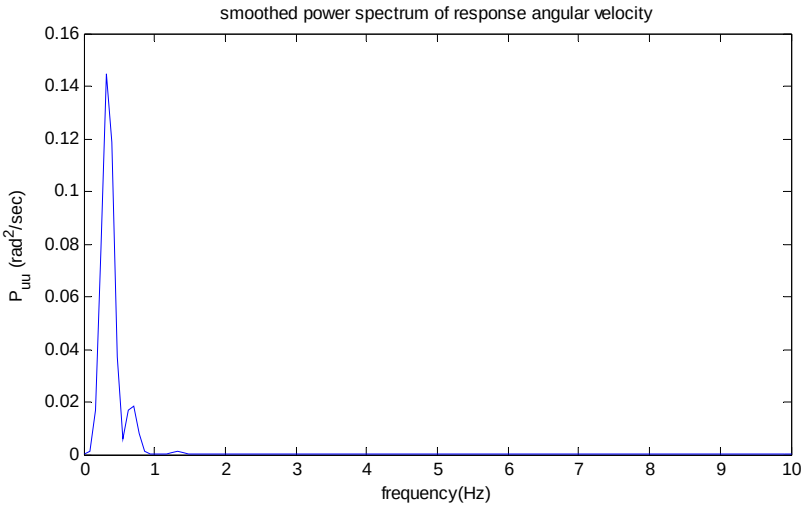

Figure 46. Power spectrum for flat plate: wave frequency =1/3 Hz

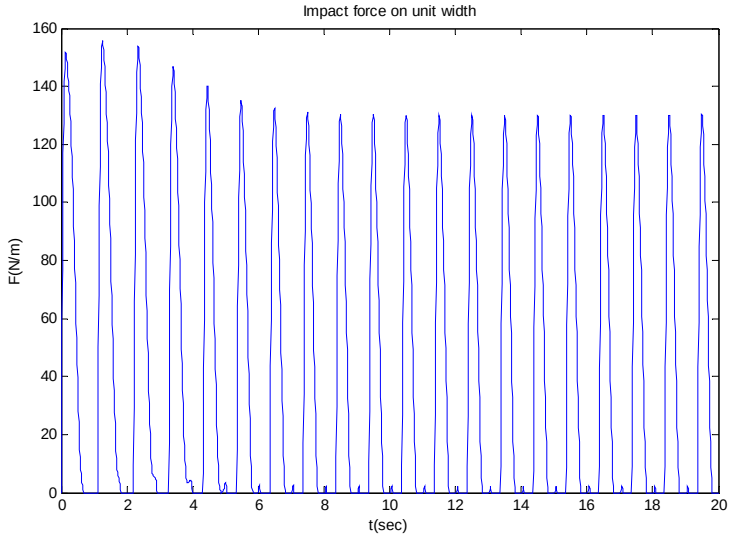

Figure 47. Impact force on plate, wave frequency= 1 Hz

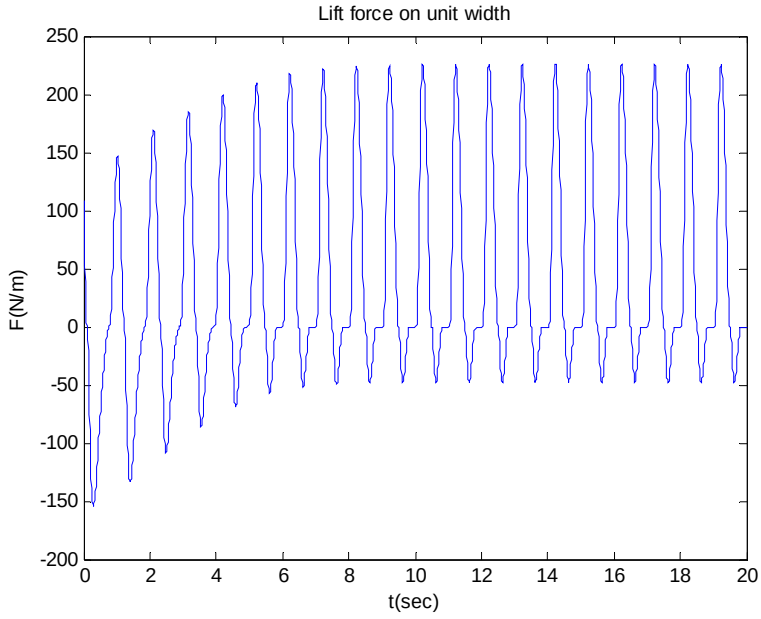

Figure 48. Lift force on plate, wave frequency= 1 Hz

3.4. Effects of modeling parameters on impact force

3.4.1. Impact velocity

To choose the proper dimensionless coefficients for setting up the experiments, a usual pendulum system with no outer forces can be used to explore the physical relationships among the variables (see Figure 49). According to the law of energy conservation, the motion of the pendulum can be written as:

$$mg\left(l-h\right)=\frac{1}{2}mv_{\max}^{2} \tag{51}$$

or

$$v_{\max}=\sqrt{2g\left(l-h\right)} \tag{52}$$

Using dimensionless variables (52) may be expressed as:

$$\frac{v_{\max}}{\sqrt{gl}}=\sqrt{2\left(1-\frac{h}{l}\right)} \tag{53}$$

It is safe to conclude that the free falling height is analytically proportional to the quadratic velocity. Figure 50 plots the quadratic relation between maximum velocity and the falling height. Figure 51 illustrates the relation between quadratic velocity and the falling height, where velocity is in form of a Froude number. In other words, free falling height and the square of impact velocity have exactly the same effects on impact force, when the pendulum impacts on water. Figure 52 and Figure 53 illustrate the relation between impact force and the quadratic impact velocity for two sphere impact models. It is found that the impact force is approximately linear with free falling height or quadratic impact velocity. Actually, the impact force is often considered proportional to the square of velocity in many previous studies.

3.4.2. Mass

When the pendulum's scales and falling height are fixed, there is no way to change them to impact velocity, but the impact force is still changeable as the mass of the pendulum changes. To avoid this disturbance from impact velocity, the effect of the falling height is removed simply by dividing impact force by quadratic impact velocity

which is linear to falling height (see Figure 54 and Figure 55). When the body penetrates the water surface, if the mass is too small, the velocity will soon reduce and the body will not penetrate deeply enough, so the impact force cannot reach a high value with the small penetrant depth and impact area. This is the reason mass affects impact force.

3.4.3. The radius of the sphere

The change of radius may update the real impact height, even though h is fixed, because the real impact height should be h minus the radius of the sphere. The result shows the radius of the sphere is linear to the impact force. The radius and the falling height have the same linear relationship with impact force. To illustrate the effect of sphere radius, the impact velocity effect is removed (see Figure 56).

3.4.4. The impact angle

The impact angle is defined as the angle between velocity and the free surface when impact is occurring. This angle is determined by the ratio of falling height and pendulum length. Generally if the ratio is low, the impact angle becomes large and the impact velocity tends to be vertical to the free surface. To illustrate the effect of impact angle, the impact velocity effect is removed. The result shows that as the impact velocity tends to be vertical, the impact force increases (see Figure 57). This result makes much sense, because an impact from the normal direction is expected to be stronger than an oblique impact.

3.4.5. The shape

Bodies of different shapes in the numerical study have presented different behaviors during wave impact. In terms of impact force, the comparison of properly defined impact coefficients of those shapes can reflect the effects of body shapes on impact force, because it makes no sense to directly compare impact force with units for completely different shapes. A widely used form of impact coefficient can be written as

$C_s = \frac{\mathrm{P}}{1/2\rho v_{impact}{}^2}$, where v_{impact} is the impact velocity. According to numerical results, the value range of C_s for each shape is generally presented in Figure 58. The sphere pendulum is subject to a larger impact, because the deadrise angle is naturally much smaller than those of the wedge and flat plate. If the wedge and flat plate experience impact on a steep wave profile, the impact loading would be large, too.

It is worth noting that the derivation of the wave impact pressure in the impact coefficient expression above may be a problem, because the value of the impact area is hard to predict and thus may deviate a great deal from the real value. There are two ways to address this problem. First, the impact area can be derived from the instant penetrant depth which is updated in each time step. The disadvantages are the pressure is impossible to distribute equally on the impact area, and the real impact area may differ from the one obtained from penetrant depth because of the free surface elevation. The other way is to skip the impact pressure, but use impact force and characteristic length to define an impact coefficient, i.e. the radius of the sphere, in the definition of impact coefficient. But this method does not work properly if we want to compare the numerical results with previous experiments, where the shapes of models are different from the numerical models in this study. That is why it is necessary to develop a new experiment of wave impact, which will be discussed in a later section.

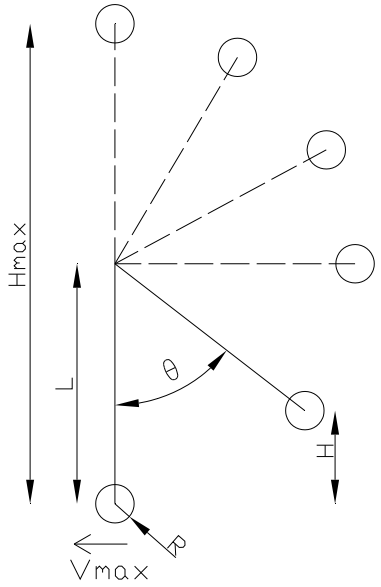

Figure 49. Variables of spherical pendulum

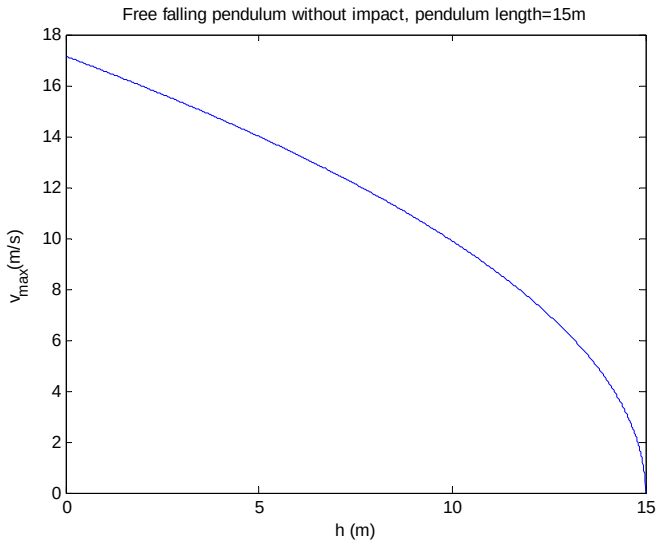

Figure 50. Analytical results of pendulum maximum velocities

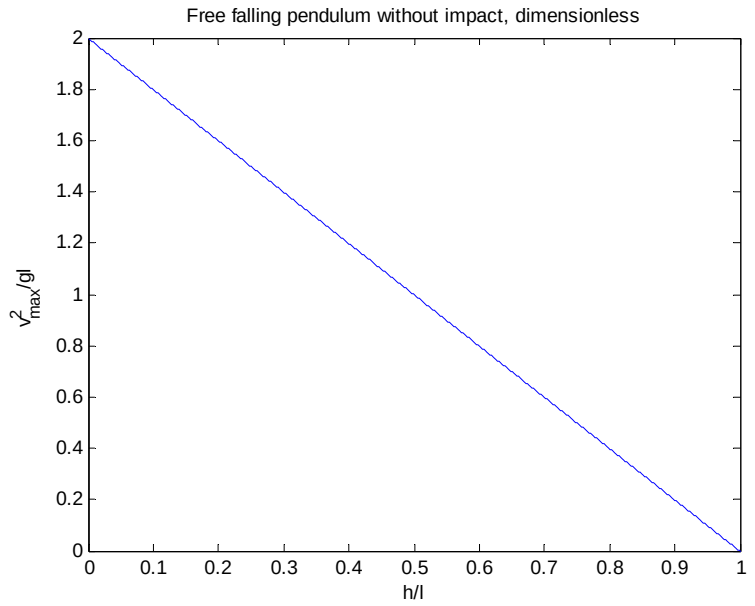

Figure 51. Square of Froude number vs dimensionless falling height

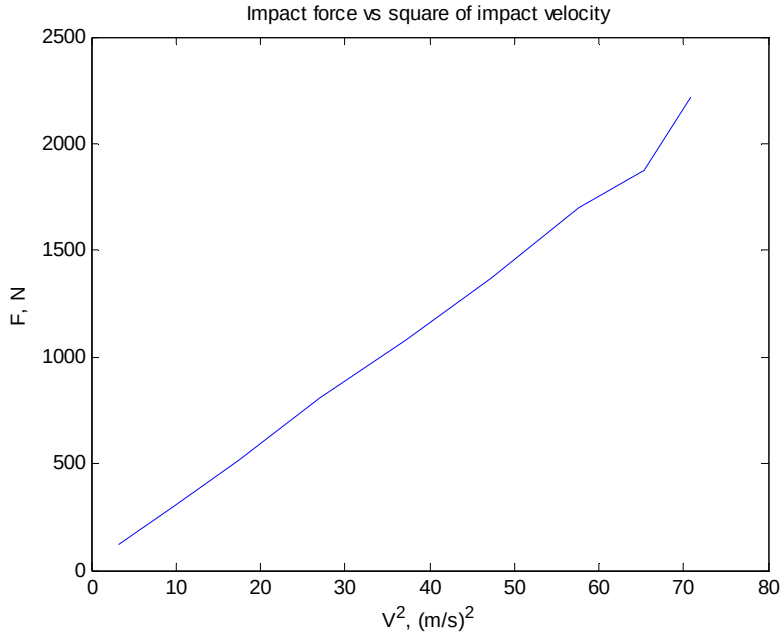

Figure 52. Numerical results for sphere pendulum, r=0.1m, l=2m, h=2m

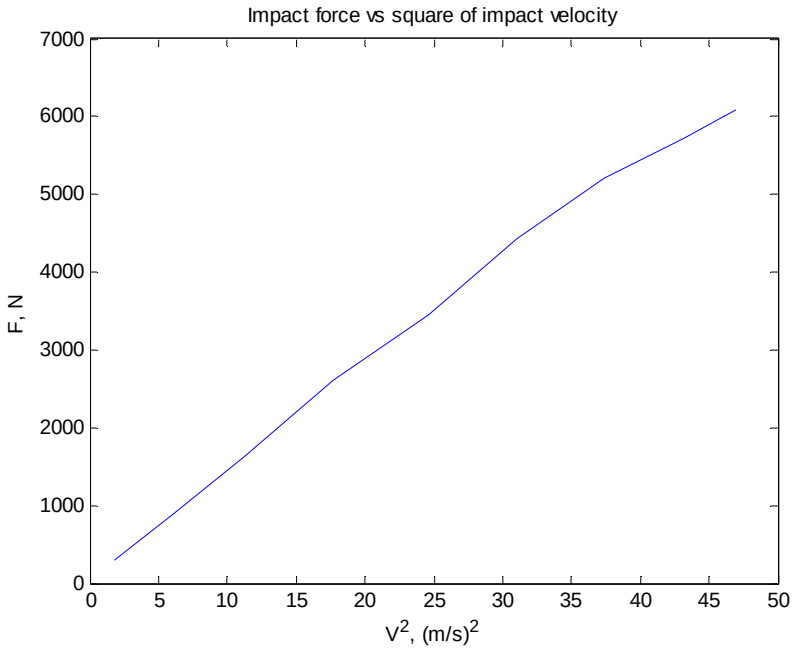

Figure 53. Numerical results for sphere pendulum, r=0.2m, l=3m, h=3m

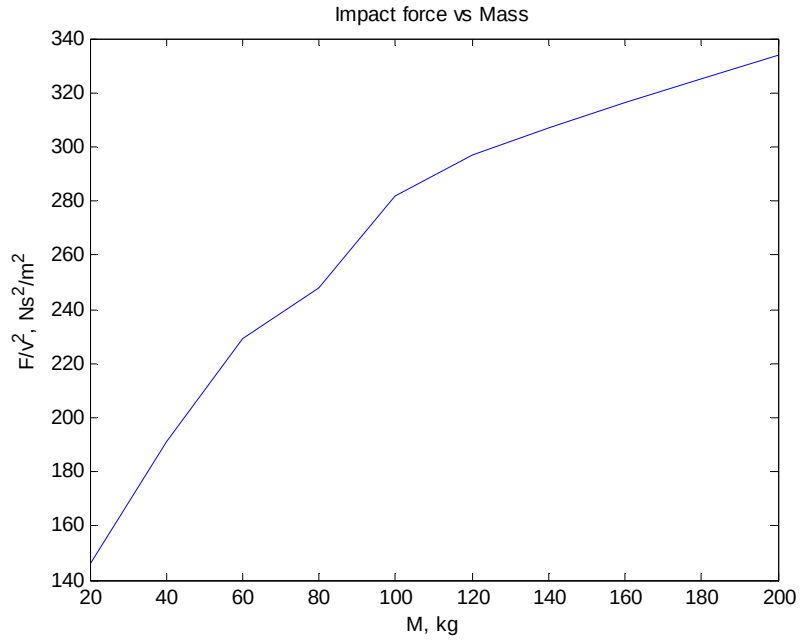

Figure 54. Effect of mass on impact force, r=0.2m, l=3m, h=3m

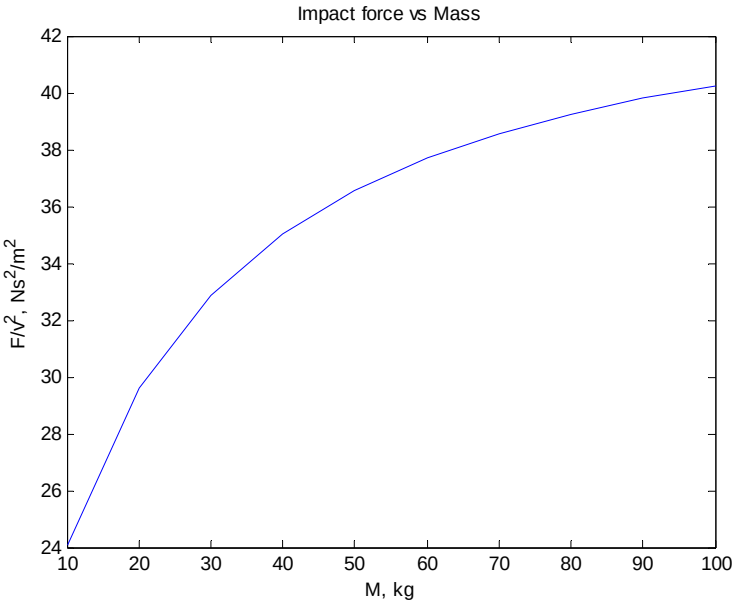

Figure 55. Effect of mass on impact force, r=0.1m, l=2m, h=2m

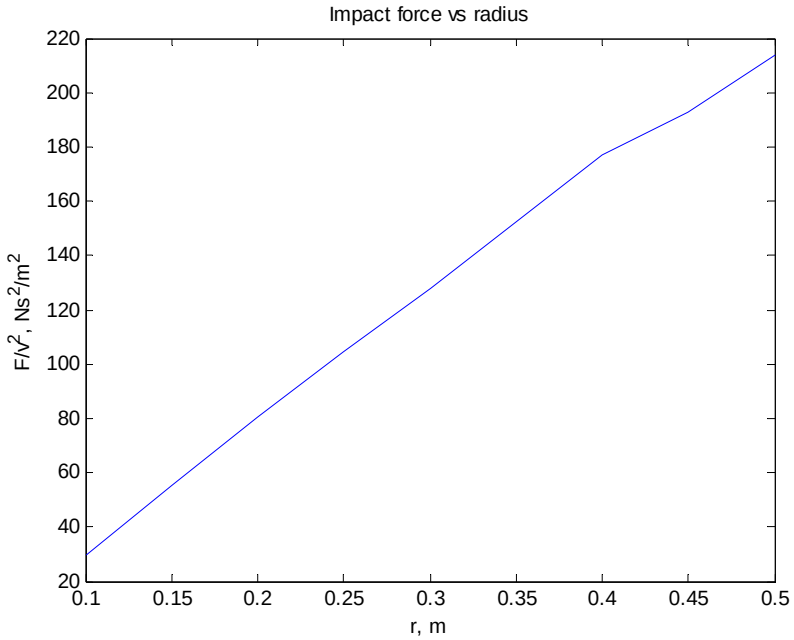

Figure 56. Numerical results for sphere pendulum, m=20kg, l=2m, h=2m

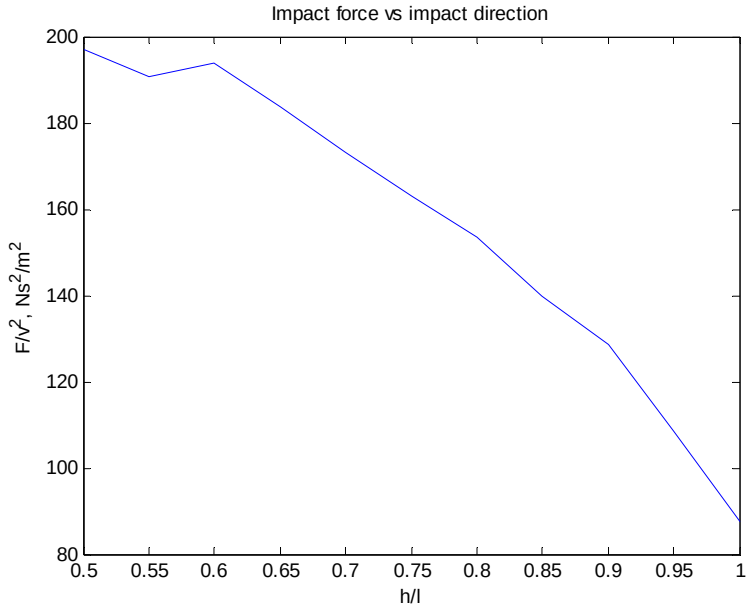

Figure 57. Numerical results for sphere pendulum, m=20kg, l=2m, r=0.2m

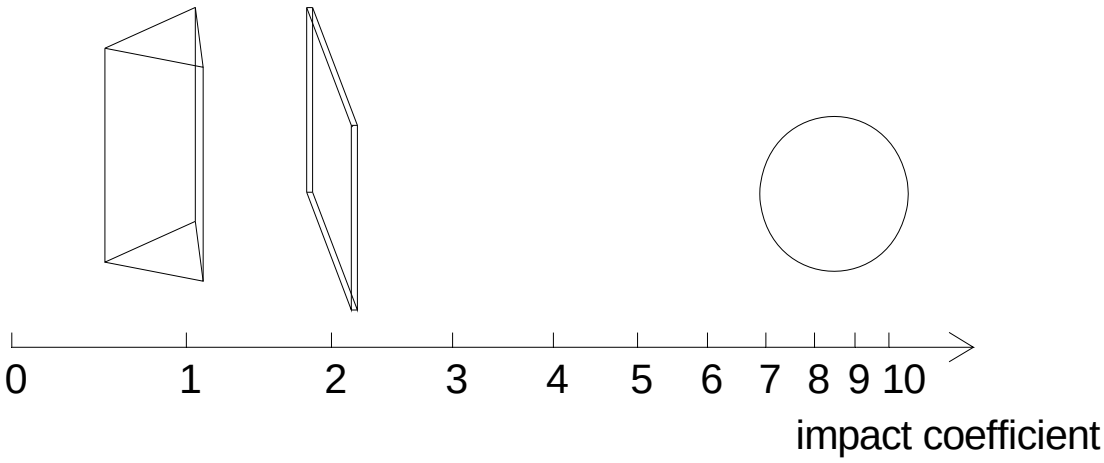

Figure 58. Impact coefficient for different shapes

3.5. Comparison with experiment

To compare the numerical results in this study with previous experiments, the first thing to do is to make sure the scale and definition of coefficients are the same. To describe the loads of real floating structures, pressure is used rather than force. The scaling ratio of pressure is the same as the scaling ratio of length under Froude's law, but it is not easy to select the proper characteristic length for a ship model to compare with the pendulum system. It has been proven that impact force is in proportion to velocity square or releasing height. Recall the slamming coefficient associated with velocity and pressure, written as $C_s = \frac{\mathrm{P}}{1/2\rho v_{impact}{}^2}$. With this coefficient, it is possible to compare the numerical result from the pendulum model with ship model tests. We choose an initial angle of $45°$, pivot height of 1.9 m, pendulum length of 2 m, which is equivalent to a falling height of 0.386 m. The impact force is 6.06×10^4 pa, and 2.74 m/s, which gives a slamming coefficient of 16.1. Now we look at actual ship loads. Yoshimoto et al. (1997) conducted an experimental investigation of a very large floating structure (VLFS), showing that the impact pressure acting on the VLFS is about $13\ tonf/m^2$ (12.75×10^4 pa) with a wave height of 8 m and wave period of 7s. The maximum wave surface velocity is $\frac{\pi H}{T} = 3.59 m/s$. The slamming coefficient with respect to pressure is then 19.8, which is close to the numerical result 16.1. Based on the slamming coefficient from the numerical model, the VLFS impact force estimated with our numerical model is:

$$6.06\times10^4\ pa\times\left(\frac{3.59 m/s}{2.74 m/s}\right)^2 = 10.40\times10^4\ pa \tag{54}$$

which is close to Yoshimoto's experimental results from ship model test 12.75×10^4 pa.

A slamming coefficient was defined by Sarpkaya (1978), written as

$$C_s = 2F/\rho DLU_m^2 \tag{55}$$

where D and L are the scales of the cylinder , DL is therefore the projected area, $U_m = 2\pi A/T$ is the maximum vertical surface raising velocity. With this definition of slamming coefficient, the results of slamming tests were up to 6.3 in Sarpakaya's tests. In initial calm water test, the velocity U_m is defined as the velocity of water entry. The slamming coefficient was from 4.1 to 6.4 in Faltinsen(1977)'s initial calm water test. The results from Sarpakaya and Faltinsen's test also coincide with the numerical results using the pendulum model, because the projected area in their definition of slamming coefficient is larger than the real impact area that use C_{sp}, the coefficient in this study.

3.6. Comparison with classification society codes

A classification society, the American Bureau of Shipping (ABS), includes rules for three different types of steel vessels: vessels intended to carry oil in bulk, vessels intended to carry ore or bulk cargos, and vessels intended to carry containers. The rules of external wave-induced bow pressure are expressed by the same equation as:

$$P_{bij} = kC_kC_{ij}V_{ij}^2 \sin\gamma_{ij} \text{ kN/m}^2 \text{ (tf/m}^2\text{, Ltf/ft}^2\text{)} \tag{56}$$

where

k = 1.025 (0.1045, 0.000888)

$C_{ij} = \{1 + \cos^2[90(F_{bi} - 2a_{ij})/F_{bi}]\}^{1/2}$

$V_{ij} = \omega_1 V \sin\alpha_{ij} + \omega_2 (L)^{1/2}$

ω_1 = 0.515 (1.68) for m (ft)

= 1.0 (1.8)

V = 75% of the design speed, V_d, in knots. V is not to be taken less than 10 knots

$\gamma_{ij} = \tan^{-1}(\tan\beta_{ij}/\cos\alpha_{ij})$, local bow angle measured from the horizontal, not to be taken less than 50°

α_{ij} = local waterline angle measured from the centerline, not to be taken less than 35°

β_{ij} = local body flat plate angle measured from the horizontal, not to be taken less than 35°

F_{bi} = freeboard from the highest deck at side to the load waterline (LWL) at Station i

a_{ij} = vertical distance from the LWL to WL_j.

C_k = 0.7 at collision bulkhead and 0.9 at 0.0125L

= 0.9 between 0.0125L and FP

= 1.0 at and forward of FP

i, j = station and waterline

The formula is analogous to the numerical result of a pendulum water impact model where the impact pressure is proportional to the squared impact velocity. The difference is V_{ij} is determined by velocity and vessel's length. The limitation of the pendulum impact model is that it can't take all naval architecture parameters into account. Besides, bottom slamming of vessels with high speed is associated with the vessel's geometry parameters, vibration frequency and design speed. However, the bottom slamming is associated with the square root of velocity rather than squared, and thus the speed's influence is much weaker than bow slamming.

The steel ships rules of Bureau Veritas (BV) give the strength requirements to resist green water forces for air pipes, ventilator pipes and their closing devices located within the forward quarter length of vessels. The green water induced pressure is given by:

$$p = 0.5 \rho V^2 C_d C_s C_p \quad (57)$$

where

ρ = density of sea water

V= velocity of water over the fore deck, recommended to be equal to 13,5 m/sec

C_d : Shape coefficient

= 0.5 for pipes

=1.3 for air pipe or ventilator heads in general

=0.8 for an air pipe or ventilator head of cylindrical form with its axis in the vertical direction

C_s =3.2, slamming coefficient

C_p: protection coefficient

=0.7 for pipes and ventilator heads located immediately behind a breakwater or a forecastle

=1.0 elsewhere and immediately behind a bulwark

The formula is consistent with the numerical result of pendulum water impact model. The air pipes and ventilator pipes are single objects not affected by naval architecture parameter. Therefore, the pendulum impact model is a good fit for the green water problems above.

In BV steel vessel rules, the bow impact pressure is given for the vessel with speed larger than 17.5 knots, length between 120m and 200m. It is expressed in kN/m^2, with the following formula:

$$p_{FI} = nC_L C_S C_Z (0.22 + 0.15\tan\alpha)(0.4V\sin\beta + 0.6\sqrt{L}) \tag{58}$$

where

C_S: coefficient depending on the type of structures on which the bow impact pressure is considered to be acting:

= 1.8 for plating and ordinary stiffeners

= 0.5 for primary supporting members

C_L: coefficient depending on the ship's length:

= 0.0125 for L < 80 m

= 1.0 for L ≥ 80 m

C_Z: Coefficient depending on the distance between the summer load waterline and the calculation point:

= C – 0.5 (z - T) for z ≥ 2 C + T - 11

= 5,5 for z < 2 C + T - 11

C : Wave parameter

α : Flare angle at the calculation point, defined as the angle between a vertical line and the tangent to the side plating, measured in a vertical flat plate normal to the horizontal tangent to the shell plating

β: Entry angle at the calculation point, defined as the angle between a longitudinal line parallel to the center line and the tangent to the shell plating in a horizontal flat plate

This formula is similar to ABS' steel vessel rules and also coincides with BV's Offshore Units rules of bow impact. The pressure is proportional to the squared speed and the vessel length.

In the Recommended Practice of Det Norske Veritas (DNV), the wave-in-deck horizontal force on the simple box-type deck structure on a fixed jack-up platform is calculated in the following formula:

$$F_h = \frac{1}{2}\rho C_h V^2 A \tag{59}$$

where, ρ is the water density, C_h=2.5 for end-on the broadside (beam and head sea), 1.9 for oblique wave (quarter sea).

The vertical upwards wave-in-deck force is then calculated by the formula:

$$F_v = \frac{1}{2}\rho C_v V_z^2 A \tag{60}$$

where, C_v=5 for end-on the broadside (beam and head sea), 10 for oblique wave (quarter sea). $\frac{F_v}{A}$ should be smaller than the peak pressure on the hull, because according to Yoshimoto's experiments, the impact pressure is not evenly distributed and the high pressure zone is only about 1/50 of the ship length, rather than the wetted area A which is indicated in the following figure. That is the reason C_v is smaller than the impact coefficient of 12 in Yoshimoto's results.

The rules also give the dynamic formula for slamming on a horizontal slender structure. The formula was first given by Kaplan and the theoretical model is very clear, rather than the semi-empirical formula raised by ABS. The vertical force per unit length of the cylinder is:

$$F_z(t) = \rho g A_1 + \left(m_{a,3} + \rho A_1\right)\ddot{\eta} + \frac{\partial m_{a,3}}{\partial z}\dot{\eta}^2 + \frac{\rho}{2}\dot{\eta}\left|\dot{\eta}\right| C_D^z(z/r) \tag{61}$$

where, the first item of RHS is the buoyancy force, the second item is Froude-Krylov force which represents the effect of the spatial pressure gradient in the waves, the third item is the impact force due to the change of added-mass, and the last term is the drag force. Similarly, the horizontal force per unit length of the cylinder is

$$F_x(t) = \left(m_{a,1} + \rho A_1\right)\dot{u} + \frac{\partial m_{a,1}}{\partial z}\dot{\eta}u + \frac{\rho}{2}u\left|u\right| h(z/r) C_D^x(z/r) \tag{62}$$

where, the velocity in (61) is changed into fluid velocity according to real impact velocity.

The slamming on vertical slender structure is calculate by the same theory, and the sectional force is eventually written as

$$F_x(z,t) = \frac{1}{2}\rho C_S D u^2 \tag{63}$$

where, C_S is the slamming coefficient,

$$C_s = 5.15\left[\frac{D}{D+19s} + \frac{0.107s}{D}\right] \tag{64}$$

where, s is the submergence relative to the wave surface.

The rules of slamming pressure over a broad plate are given by

$$p_s = \frac{1}{2}\rho C_{pa} v^2 \tag{65}$$

where, v is the relative normal velocity between water and surface, and the slamming coefficient is given by

$$C_{pa} = \frac{2.5}{\left(\tan\beta\right)^{1.1}} \tag{66}$$

From DNV's rules of slamming, it is not difficult to figure out that they are based on the classic von Karman's theory that the force due to impact is calculated from the timely change of added-mass induced momentum, and for a slender structure, Morison's equation is applied. The theories in DNV's rules are consistent with the theory used in

our pendulum impact model, and our numerical results are consistent with DNV's formulae, that the impact pressure is proportional to the squared impact velocity.

4. EXPERIMENT DESIGN

So far the numerical results of the impact of the pendulum system have been presented and compared with previous experiments on wave impact problems. However, none of the previous experiments use a pendulum model, so the comparison between numerical results in this study and previous experimental results is only approximate and qualitative. On the other hand, most previous experimental results are in terms of impact pressure and it is not quite precise to convert the numerical results from force to pressure in the numerical study. For a more reliable comparison between numerical results and experimental data, a hydrodynamic experiment of wave impact on pendulum system in wave flume was designed, so that the uniform definition of an impact coefficient can be utilized to compare the numerical and experimental results.

4.1. Similarity and scaling considerations

To design a hydrodynamic model test, dimensionless numbers are used to scale the parameters of the model to make the experimental model dynamically similar to the prototype. The Reynolds number, the Froude number, the Strouhal number and the Euler number are considered most commonly in model tests. Theoretically, in hydrodynamic tests only when all four numbers are equal for model and prototype, is the model said to be similar to the prototype, but it is nearly impossible to set up such an experiment. The Reynolds number concerns the viscosity of the fluid, so if the viscous drag force dominates, the Reynolds number is used for scaling variables related to viscosity in the test. The Froude number is used where the inertia force dominates. The Strouhal number involves the unsteady motion of fluid, and is often applied in vortex induced vibration problems. The Euler number reflects the effect of compressibility. In the impact problem, the drag is quite small relative to the inertia impact force, and vorticity and compressibility are neglected. Therefore the scale ratios should be determined by laws of Froude. Table 6 is developed for the Froude number as the scale criterion. Gravitational

acceleration g and fluid density ρ are constants in the scaling. Table 7 is an example of scaling a sphere with scaling ratio 1/10.

The scaling ratio between the real ship and a pendulum model should be determined by the capability of an experimental device, specifically, the wave maker. For example, if the ratio of the wave height in wave flume and the real wave height is determined, this ratio is set as the scaling ratio, and other scaling ratios are calculated based on it, according to Froude's law.

4.2. Dimensionless parameters

The data of a hydrodynamic experiment should be presented in terms of dimensionless coefficients that do not depend on units and the scaling ratio of the model. Proper dimensionless coefficients should be chosen from a scaling analysis based on the qualitative relationship between the variables known from the numerical analysis, which are summarized in Table 8.

The impact pressure is a function of impact angle δ, impact velocity, body mass, body size, fluid density and the shape of model, written as

$$F_{impact} = f(\delta, v, m, \rho, r, shape) \tag{67}$$

Using π theorem, Eq (68) can be written as

$$\frac{F_{impact}}{\frac{1}{2}\rho v^2 r^2} = f(\delta, \frac{m}{\rho r^3}, shape) \tag{69}$$

where the LHS is defined as the impact coefficient, as in many studies on wave impact. It is worth noting that under the same Fr, impact pressure varies by the same ratio as the characteristic length, which coincides with Fr number's scaling rules in Table 8.

Table 6. Scaling ratio of Froude numbers

Parameter	Dimension	Scale ratio($r = \frac{L_{model}}{L_{prototype}}$)
Length	L	r
Time	T	$r^{1/2}$
Mass	M	r^3
Velocity	LT^{-1}	$r^{1/2}$
Acceleration	LT^{-2}	-------
Angle	-------	-------
Angular velocity	T^{-1}	$r^{-1/2}$
Frequency	T^{-1}	$r^{-1/2}$
Force	MLT^{-2}	r^3

Table 7. The scaling for an exemplary sphere model

Parameters input	prototype	ratio	Model
Mass	20000kg	1/1000	20kg
Length of pendulum	100m	1/10	10m
Radius	10m	1/10	1m
Wave height	5m	1/10	0.5m
Wave period	6sec	$\sqrt{1/10}$	1.9sec

Table 8. Properties of modeling variables

Variables	Peak impact pressure	Response of dynamic system
L	\	Natural period, exciting moment
m	\	Natural period, inertia
h(θ)	Impact pressure	Initial conditions
Shape(sphere, wedge, flat plate, hemisphere)	Impact pressure	Hydrodynamic coefficients
r(dimension of objects)	Duration of impact, impact force	Magnitude and duration of exciting force
Impact angle	Impact pressure	\

The impact forces in our models are defined in terms of moments, with respect to the pendulum's pivot. The wave impact coefficient for the sphere is defined as

$$C_{imp} = \frac{M_{total}}{l\rho r^2 v^2} \tag{70}$$

where M_{imp} represents the impact inducing global moment of the numerical results, l is the length of pendulum, r is the characteristic size of the body, and v is impact velocity.

Using the impact coefficient in either of the recommended forms above, the important relationships, C_{imp} vs shape, C_{imp} vs $\frac{m}{\rho r^3}$ and C_{imp} vs δ, can be investigated through experimental studies. This represents a major goal of this experimental study. As long as those relations are exactly known, it is possible to design pendulum models to simulate dynamic impact system with any impact coefficients.

For the impact on wave profile, rather than initial calm water, the impact coefficient also can be defined with a characteristic velocity, $H/2\omega$, the maximum surface raising velocity. The impact coefficient can then be expressed as

$$C_{imp} = \frac{M_{total}}{l\rho r^2 (H/2\omega)^2} \tag{71}$$

With this definition of impact coefficient, the relationship between C_{imp} and impact velocity can be investigated, even though it is already understood quite clearly, both numerically and theoretically.

4.3. Conceptual design of the apparatus

A series of tests on a pendulum system was designed in order to develop an effective experimental apparatus to simulate wave slamming in the real world, as well as to compare with the numerical results. The tests are conducted in the Ocean Engineering Wave Tank at Texas A&M University. The 2D wave tank is 35.05 meters long, 0.914 meters wide and 1.22 meters deep, with glass walls and a beach wave absorber. A variable height random deepwater wave generator is able to generate wave heights of

0.254 meters in 0.914 meters of water. The towing carriage is mounted on rails and is capable of driving at a maximum speed of 0.610 m/s. For each body shape, a series of tests involve models with different wave frequencies, initial falling heights, and pendulum lengths. To serve this purpose, a pivot height adjustable pendulum device with a PVC hollow arm was designed, as illustrated in Figures 59 and 60. The pivot height can be adjusted by sliding the ends of the triangle tower's legs along the rail. A variable weight can be attached to the arm at a variable position, which can both change the natural frequency and the mass of the pendulum. This design saves effort in preparing arms with different lengths and bodies with different masses. Table 9 presents the scales of the pendulum model properties for the experiment setup. A speedometer is mounted to a specific height and follows the movement of the pendulum. The tip of the speedometer is always attached to a smooth pad mounted on the pendulum arm at the same height as the speedometer, as soon as the pendulum falls to a low enough height. Pressure sensors are mounted on the bodies. Figure 61 is an example of a pressure sensor pattern on the spherical body. The pressure sensor wires go from the inside of the body through the inside of the hollow arm and reach to the top of the triangle tower. A wave height sensor is used to make sure the desired waves are generated.

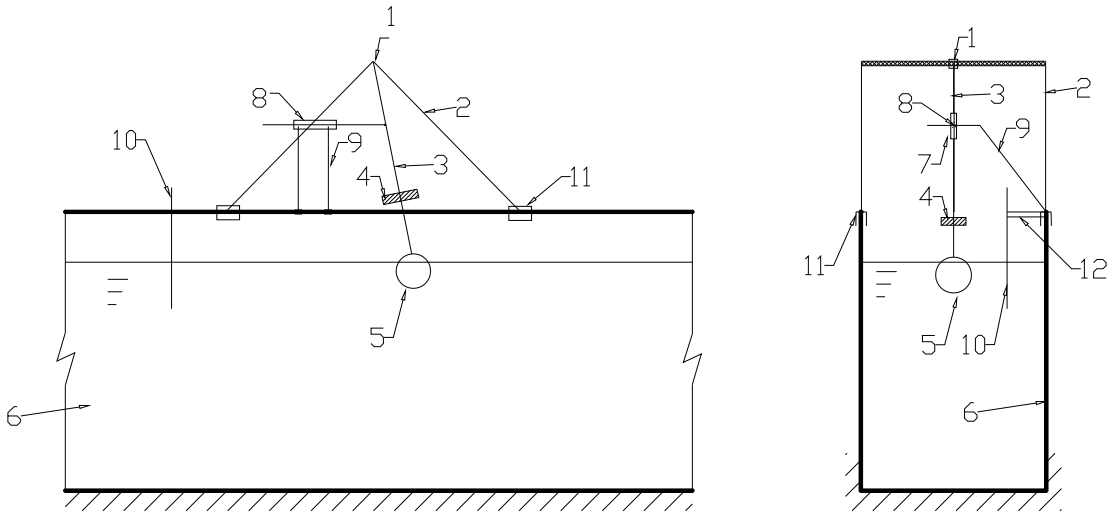

Figure 59. Plan of experiment setup

1--- Frictionless pivot	2--- Triangle tower	3--- Light pole
4--- Control weight	5--- Pendulum bob	6--- Water flume
7--- Smooth pad	8--- Movement transducer	9--- Transducer shelf
10--- Wave height sensor	11--- Adjustable fixer	12--- Wave sensor shelf

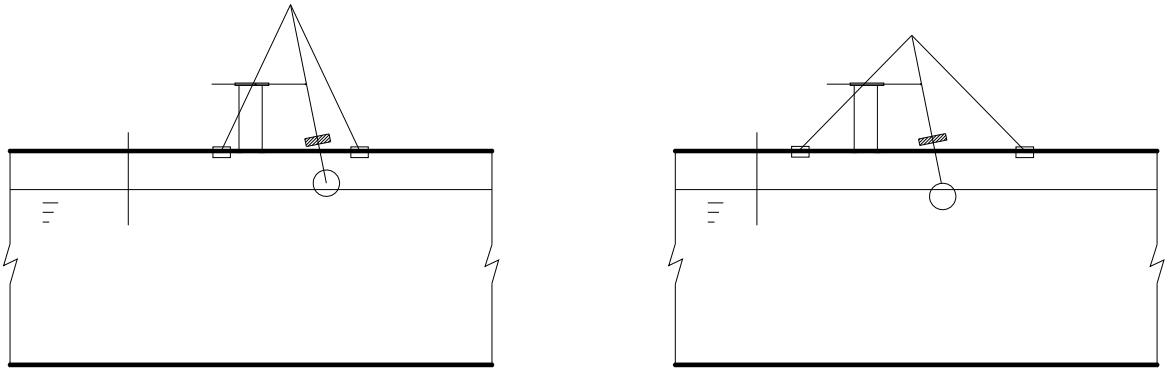

Figure 60. Adjusting pivot height by sliding fixers of triangle tower

Table 9. Parameter selecting of experiment setup

Properties	*Value*	*Units*
PVC Arm length	1.0	M
PVC Arm diameter		
Inner	1.5	CM
Outer	2.5	CM
Triangle legs length	0.9	M
Height of movement transducer	0.5	M
Water depth	1.02	M
Mass of weight	3.0	Kg
Mass of body	Various	
Dimension of body	Various	

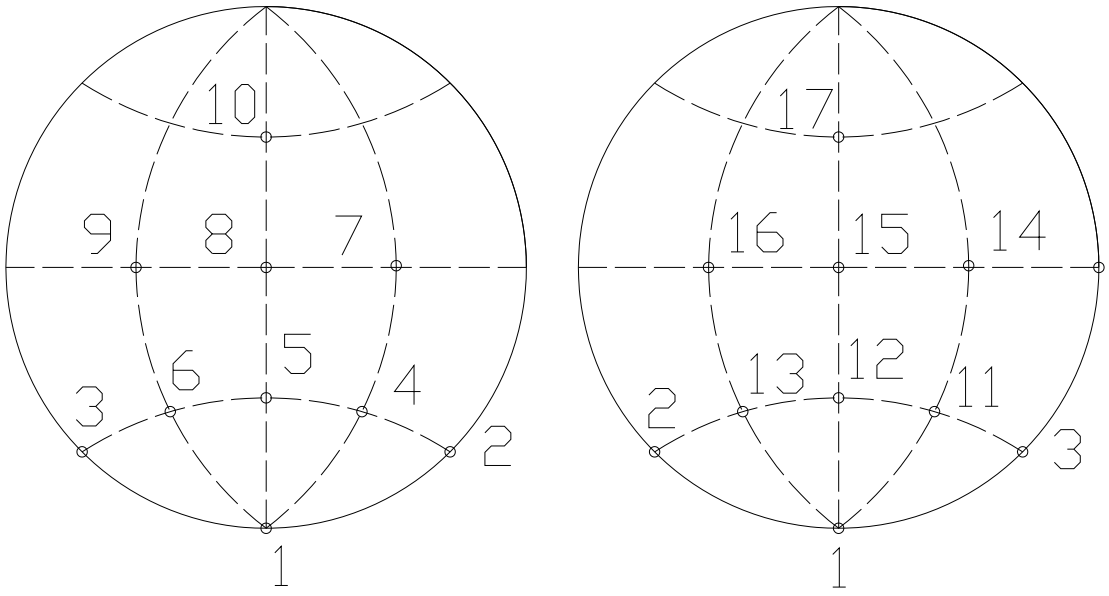

Figure 61. Pressure transducer positions

5. CONCLUSION

A wave impact model based on the development of a pendulum system was studied to verify its capability to simulate slamming loads on offshore structures and vessels. The wave impact force and the dynamic behavior of the model was investigated using numerical simulations and results were compared with previous experimental data and classification society design codes. A basic experimental design of a pendulum apparatus was developed in order to provide a first look at a device that could be used to measure impact loads.

The essence of this wave impact model is a single degree-of-freedom pendulum system described in terms of angular motion. The system is excited by wave forces acting on the body, which is fixed to the end of the pendulum. The usual wave forces are evaluated by Morison's equation, and the impact force is estimated by von Karman's method. Hydrodynamic coefficients are mainly obtained from existing experimental data. Since the exciting forces are related to the motion of systems and include several nonlinear terms, the 4th order Runge-Kutta time domain ordinary differential equation solver is used to solve the equation of motion and obtain the time history of motion.

Three body shapes, sphere, flat plate and vertical triangular body, were used in the numerical investigation of wave impact force since the loads are highly dependent on body shape. The pendulum system displays different dynamic behaviors when subject to different wave frequencies. In the numerical simulation, the wave frequencies were varied between 1/3 Hz to 2 Hz, and the pendulum system natural frequency was 0.35 Hz. These were close to the ocean wave and compliant structural frequencies obtained based upon Froude number scaling. For the sphere, the natural frequency and exciting frequency were not shown in the response spectrum when it encountered high wave frequencies, due to strong nonlinear behavior. Because a nonlinear von Karman impact force comprises a larger portion of the total force than for other shapes, the numerical prediction can be less accurate. On the other hand, at lower excitation frequencies, the natural frequency dominates the response spectrum, consequently the loads imposed on

the system can be considered to be an impulsive excitation and results in free vibration at the natural frequency. In a special case where the sphere remains completely submerged in water, the response demonstrates a more linear behavior. The spectrum is then simply made up by natural frequency and wave frequency, because of the absence of impact on wave profile. Without the abrupt impact, the nonlinear behavior is weakened and the system experiences continuous force loading rather than impulse loading.

For the vertical triangular body, the impact force exerted on the structure is less sudden and less fierce than that on the sphere. This leads to a response spectrum that follows linear dynamics theory. The power spectrum clearly displays the natural frequency, the exciting wave frequency and various harmonics. At the resonant frequency, the response amplitude remains at a high value, because of the low damping force contribution from the viscous drag force.

For the plate body, the outstanding property of response is the large inertia force. Due to a great amount of lift, the plate cannot restore itself to its original position when subject to high wave frequencies. The natural frequency is difficult to observe in the response spectrum, because the large lift force serves as damping in the system. Wave frequency dominates the power spectrum for most frequencies. At the resonant frequency, the response is still at a normal magnitude. In other words, for the plate body, the natural frequency is dominated by the large time-dependent damping force, and to some extent, the system loses its dynamic feature. Though the systems of the vertical triangular body and plate body also experience impact force, this impact force, as well as other wave forces, is gradual and continuous. Thus, the nonlinearity of wave forces is too weak to be observed from response plots. In conclusion, the shape of the body influences the dynamic behavior mainly by changing the proportion of each force component, while the properties of wave force components are different.

The peak impact force is shown to be affected by several modeling parameters, including impact velocity, mass, body radius, impact angle and shape. Impact velocity is the most important factor affecting impact force, such that the impact coefficients in most previous studies are defined by the relationship between impact force and impact

velocity. In this study, the plots of quadratic impact velocity versus the peak impact force show that quadratic impact velocity is approximately linearly related to the peak impact force. Impact velocity is the maximum velocity at which a pendulum falls to the water surface. It is also shown analytical that the falling height is proportional to the quadratically to the maximum velocity; therefore, falling height is linear to impact force. The falling height, or the quadratic velocity, is actually equivalent to the energy released during the impact.

Body mass is not associated with velocity, but it is still found that increasing mass causes the peak impact force to increase, especially when the mass is small. One explanation is that when the mass is too small, the body does not have enough energy to penetrate the water. A light body can be easily bounded back before it reaches a large impact force value. The radius of a body is also found to be approximately linearly related to the peak force. This is unexpected, considering the impact area is proportional to the square of the radius. However, a large radius leads to a less deep penetration, similar to the effect of a smaller mass. The impact angle or direction is another important factor of impact force. In calm water, the value of falling height over pendulum length determines the impact angle. When the direction of impact velocity is perpendicular to the free surface, the impact force reaches the greatest value. For the same reason, the impact force in the front of a body is very large in a high sea condition, because a steep crest results in an impact angle close to a right angle.

Moreover, the shape of the body is seen to influence the impact force or, from a dimensionless perspective, the impact coefficient. Body shape influences the interaction between body and water. For instance, the vertical triangular body has a smaller impact coefficient, because it has a sharp shape to pierce the profile. Also, continuous contact with water leads to a smaller impact coefficient on the plate than on the sphere, which penetrates water from the air. These facts are consistent with naval architecture real world design practice. For example, a vessel designed with a sharp bow can reduce the impact force when it heads into big waves and a large impact is exerted on the bottom when a high speed vessel lifts out of the water and falls to water again.

Comparing the numerical results with previous experiments and existing codes leads to a qualitative verification of the capability of the numerical model. Thus, this study has basically shown the pendulum model to be an effective and efficient method to predict the slamming effect on ocean structures. This is especially so for a high-speed vessel running into waves, where the relative motion between vessel and water is similar to the pendulum impact model. However, based on available experimental data, it is difficult to make an accurate quantitative comparison between the pendulum model and previous studies, due to the lack of data of any similar pendulum model. This research study has illustrated the feasibility of using the pendulum model as a robust method on wave slamming problems. Some effort was directed toward designing an experimental setup to utilize the pendulum model concept for use in studying on wave slamming loads. Further research that includes experimental studies is needed to establish the pendulum system as design tool for studying impact loads on ships and offshore platforms.

REFERENCES

Aquelet, N., Souli, M., Olovsson, L. 2006. Euler-lagrange coupling with damping effects: application to slamming problems. Computer Methods in Applied Mechanics & Engineering, 195 (1-3), 110-132.

Boccotti, P. 2000. Inertial wave loads on horizontal cylinders: a field experiment. Ocean Engineering, 23 (7), 629-648.

Chakrabarti, S. K. 1987. Hydrodynamics of Offshore Structures. WIT Press, Billerica MA.

Chakrabarti, S. K. 2005. Handbook of Offshore Engineering. Elsevier, Maryland Heights, MO.

Campbell, I. M. C., Weynberg, P. A. (1980). Measurement of parameters affecting slamming. Final Report, Rep. No. 440, Technology Reports Centre No. OT-R-8042. Southampton University, Southampton, UK.

Chen, H., Yu, K. 2009. CFD simulations of wave-current-body interactions including greenwater and wet deck slamming. Computers & Fluids, 38 (5), 970-980.

Chuang, S. L. 1967. Experiments on slamming of wedge-shaped bodies. J. Ship Research, 11, 190-198.

Faltinsen, O.M., Kjærland O, Nøttveit A, Vinje T. 1977. Water impact loads and dynamic response of horizontal circular cylinders in offshore structures. In: Proc. 9th Annual Offshore Technology Conference, 1, Houston, TX, 119–25.

Faltinsen, O.M. 1990. Sea Loads on Ships and Offshore Structures. Cambridge University Press. Cambridge, UK.

Faltinsen, O.M., Landrini, M., Greco, M. 2004. Slamming in marine applications. Journal of Engineering Mathematics, 48, 187-217.

Greco, M., Colicchio, G., Faltinsen, O.M. 2008. Bottom slamming for a very large floating structure: uncoupled global and slamming analyses. Journal of Fluids and structures, 25, 406-419.

Greenhow, M. 1987. Wedge entry into initially calm water. Applied Ocean Research, 9 (4), 214-233.

Hermundstad, O.A., Moan, T. 2005. Numerical and experimental analysis of bow flare slamming on a Ro-Ro vessel in regular oblique waves. Journal of Marine Science and Technology, 10, 105-122.

Isaacson, M., Prasad, S. 1994. Wave slamming on a horizontal circular cylinder. International Journal of Offshore and Polar Engineering, 4(2), 81-88.

Kaplan, P., Silbert, M. N. 1976. Impact forces on platform horizontal members in the splash zone. In: Proc. Offshore Tech. Conf. OTC 2498, Houston, TX, 749-758.

Korobkin, A. 1996. Theory and numerical methods for the hydrodynamic analysis of marine Hydrodynamics. Comp. Mech. Publ, 323-371.

Le Sourne H., Couty N., Besnier F., Kammerer C., Legavre H., 2003. LS-DYNA applications in shipbuilding. 4th European LS-DYNA Users Conference. Plenary Section 2, Ulm, Germany.

Liaw, C. Y. 1996. Bifurcation behaviour and wave slamming force on a compliant horizontal cylinder. Engineering Structures, 18 (9), 675-684.

Oger, G., Doring, M., Alessandrini, B., Ferrant, P. 2006. Two-dimensional SPH simulation of wedge water entries. Journal of Computational Physics, 213, 803-822.

Oliver, J. M. 2007. Second-order Wagner theory for two-dimensional water-entry problems at small deadrise angles. J. Fluid Mech, 572, 59-85.

Peseux, B., Gornet, L. Donguy, B. 2005. Hydrodynamic impact: numerical and experimental investigations, Journal of Fluids and Structures, 21, 277-303.

Rahman, M., Bhatta, D.D. 1993. Evaluation of added mass and damping coefficient of an oscillating circular cylinder. Appl. Math. Modelling, February, 17, 70-79.

Sarpkaya, T. 1978. Wave impact loads on cylinders. In: Proc. Offshore Tech. Conf, OTC 3065, Houston, TX, 169-176.

Sarpkaya, T., Isaacson, M. 1981. Mechanics of Wave Forces on Offshore Structures. Van Nostrand Reinhold, New York.

Suchithra, N., Koola, P.M. 1995. A study of wave impact on horizontal slabs. Ocean Engineering, 22 (7), 687-697.

von Karman, T. 1929. The impact of seaplane floats during landing. NACA TN 321.

Wagner, H. 1932. Über stoss- und gleitvorgange an der oberfläche von flüssigkeiten. ZAMM 12, 192–235.

Wheeler, J.D. 1969. Method for calculating forces produced by irregular waves. In: Offshore Technology Conference, Houston, Texas, 1, 71–82.

Yoshimoto, H., Ohmatsu, K., Ohmatsuandi, S., Ikebuchi, T. 1997. Slamming load on a very large floating structure with shallow draft. Journal of Marine Science and Technology, 2, 163–172.

Zhao, R., Faltinsen, O.M. 1993. Water entry of two-dimensional bodies. J. Fluid Mech, 246, 593–612.

Zhao. R., Faltinsen, O.M., Aarsnes, J. 1997. Water entry of two-dimensional sections with and without flow separation. 21th Symposium on Naval Hydrodynamics, Trondheim, Norway, 408-423.

APPENDIX A

Nomenclature

a	=	wave amplitude
A_{33}	=	vertical component of added-mass
B	=	global damping coefficient
c	=	wave celerity
C_a	=	added-mass coefficient
C_d	=	nonlinear coefficient
C_s	=	slamming coefficient
d	=	water depth
D	=	characteristic scale of body
g	=	gravitational acceleration
H	=	wave height
K	=	global stiffness coefficient
L	=	wave length
m	=	mass of pendulum body
m_{added}	=	added-mass of pendulum body
R	=	radius of pendulum body
s	=	vertical coordinate with respect to water bottom
T	=	wave period
u	=	horizontal water particle velocity
$\dot{u}$	=	horizontal water particle acceleration
u_r	=	particle velocity relative to structural velocity
v	=	vertical water particle velocity
$\dot{v}$	=	vertical water particle acceleration
x, y	=	global coordinate

η = wave elevation

ρ = water density

ϕ = wave velocity potential

θ = wave phase

ω = angular wave frequency

APPENDIX B

MATLAB™ CODES FOR SPHERICAL BODY

1. Spherical body impact dynamic equations

```
function [th_prime F1 F2 F3]= sphere_stretching(t, th)
th_prime=zeros(2,1);          % define output vector

%%%%%%%%%%%%% INPUT  PARAMETERS %%%%%%%%%%%%
scl=1;                        % scale ratio
m=50*scl^3;                   % mass,kg
l=2*scl;                      % length of pendulum,m
h=2*scl;                      % pivot height,m
r=.1*scl;                     % radius of sphere,m

g=9.81;                       % gravity acceleration,m/s^2
H=0.2*scl;                    % wave height,m
d=5*scl;                      % water depth,m
T=2*scl^0.5;                  % wave period,s
den=1.027e3;                  % water density,kg/m^3
cm=1.20;                      % added-mass coefficients
c3=0.042;c4=12.754;           % f-k force coefficients from handbook

w=2*pi/T;                     % angular frequency,1/s
k=w^2/g;                      % wave number,1/m
c=w/k;                        % wave celerity,m/s
x=sin(th(2))*l;               % x-coord of sphere center
y=h-cos(th(2))*l;             % y-coord of sphere center
el1=H/2*cos(k*x-w*t);         % wave elevation for the lowest point
dela=-k*H/2*sin(k*x-w*t);     % slope of water surface
a=-atan(dela);
```

```
hd=h-cos(th(2))*l-r;        % y-coord of low point
hu=h-cos(th(2))*l+r;        % y-coord of high point

if hu<el1                   %full immersed condition, high point is under wave profile
   V=4/3*pi*r^3;            % volume of sphere

   %added inertia
   am_surge=0.5*den*g*V;  % added-mass for surge motion
   am_heave=0.5*den*g*V;  % added-mass for heave motion
   ja=am_surge*sin(th(2))+am_heave*cos(th(2))*l^2; % inertia due to added-mass

   %f-k force
   ph=k*x-w*t;         % phase
   s=y+d;              % y-coord wrt water bottom
   el=H/2*cos(ph);     % water elevation
   u=g*k*H/2/w*cosh(k*s)/cosh(k*(d+el))*cos(ph);     % horizontal particle velocity
   v=g*k*H/2/w*sinh(k*s)/cosh(k*(d+el))*sin(ph) ;    % vertical particle velocity
   ax=g*k*H/2*sin(ph);                               % horizontal particle acceleration
   ay=-g*k*H/2*sinh(k*s)/cosh(k*(d+el))*cos(ph);     % vertical particle acceleration
   mfk=1.5*den*V*ax*l;
   mimp=0;                                % moment of impact force
   fimpc=0;                               % resultant impact force
   Fc=sqrt((1.5*den*V*ax)^2+(1.1*den*V*ay+den*V*g)^2);       % resultant total force
   lal=0;                                 % impact pressure

elseif hu>el1 & el1>y       % mostly immersed condition, center is under wave profile
   dims=(el1-y)*cos(a)+r;   % calculate d accurately
   %immersed inertia
   am_surge=0.5*den*g*vol_sph(r,dims);
   am_heave=0.8*den*g*vol_sph(r,dims);
   ja=am_surge*sin(th(2))*l^2+am_heave*cos(th(2))*l^2;
   %f-k force
```

```
    V=vol_sph(r,dims);        %immersed volume
    ph=k*x-w*t;
    el=H/2*cos(ph);
    s=y+d;                    % use sphere center as center of submerged volume
    u=g*k*H/2/w*cosh(k*s)/cosh(k*(d+el))*cos(ph);  % particle velocities at surface
    v=g*k*H/2/w*sinh(k*s)/cosh(k*(d+el))*sin(ph);

    ax=g*k*H/2*sin(ph);
    ay=-g*k*H/2*sinh(k*s)/cosh(k*(d+el))*cos(ph);
    %f-k force by coefficients and immersed volume
    mfk=1.5*den*V*(ax+c3*w*v)*cos(th(2))*l+1.1*den*V*(ay+c4*w*u)*sin(th(2))*l;
    mimp=0;
    fimpc=0;
    Fc=sqrt((1.5*den*V*(ax+c3*w*v))^2+(1.1*den*V*(ay+c4*w*u)+den*V*g)^2);
    lal=0;
else
    n=500;                    % number of discrete elements
    xdom=linspace(x-r,x+r,n);  %the horizontal domain of object
    span=2*r/n;               % horizontal span
    alld=[];                  % collection of discrete immerse depth
    I=[];
    tipt=h-l*cos(th(2));      %y coord of most left point
    for i=1:n
        eli=H/2*cos(k*(xdom(i))-w*t);
        dx=span*(i-1);
        dtip=sqrt(r^2-(r-dx)^2);
        tip=tipt-dtip;
        if eli> tip
            alld=[alld,eli-tip];
            I=[I,i];
        end
    end
```

```
  if  length(alld)==0       % not immersed
      fimpc=0;
      ja=0;
      fimpx=0;
      mfk=0;
      mimp=0;
      Fc=0;
      dV=0;
      dd=0;
      V=0;
      lal=0;
  else                      % slightly immersed

      xdom_mid=xdom(ceil(median(I)));    % x-coord of the center of submerged area
      ev=H/2*w*sin(k*xdom_mid-w*t);    % velocity of surface elevation at the middle of
immersed area
      dela=-k*H/2*sin(k*xdom_mid-w*t);  % slope of waterline
      a=-atan(dela);
      dmid=alld(ceil(length(alld)/2));          % the center component of alld
      dmax=max(alld);                           % the maximum component of alld
      dims=mean([dmid,dmax])*cos(a);       % submerged depth
      V=vol_sph(r,dims);
      dt=0.002;                                 % time lag, to get derivation of V
      dd=-sin(th(2))*th(1)*l*dt;                % often less than 0
      dV=(vol_sph(r,dims+dd)-V)/dt;          % immersed volume changing rate
      fimpx=0.8*den*g*dV*(c-th(1)*l*abs(cos(th(2))));          % horizontal impact force
      fimpy=0.8*den*g*dV*(ev-th(1)*l*abs(sin(th(2))));         % vertivcal impact force
      mimp=fimpx*abs(cos(th(2)))*l+fimpy*abs(sin(th(2)))*l; % impact moment
      fimpc=sqrt(fimpx^2+fimpy^2)*sign(th(2));                  % resultant impact force, with
direction correction!
      simp=(r^2-(r-dims)^2)*pi;                                 % impact area (projected)
      lal=fimpc/simp;
```

```
    if  dd<0                    % when exit
       mimp=0;
       fimpc=0;
       fimpx=0;
       fimpy=0;
    end

    am_surge=0.5*den*g*vol_sph(r,dims);                    % added-mass
    am_heave=0.8*den*g*vol_sph(r,dims);
    ja=am_surge*sin(th(2))*l^2+am_heave*cos(th(2))*l^2; % added inertia
    ph=k*xdom_mid-w*t;                    % wave theory, calculate f-k force
    el=H/2*cos(ph);
    s=d+el;                                % use velocities at wave surface
    u=g*k*H/2/w*cos(ph);

    v=g*k*H/2/w*sinh(k*s)/cosh(k*(d+el))*sin(ph);
    ax=g*k*H/2*sin(ph);
    ay=-g*k*H/2*sinh(k*s)/cosh(k*(d+el))*cos(ph);
%f-k force
    mfk=1.5*den*V*(ax+c3*w*v)*cos(th(2))*l+1.1*den*V*(ay+c4*w*u)*sin(th(2))*l;

Fc=sqrt((1.5*den*V*(ax+c3*w*v)+fimpx)^2+(1.1*den*V*(ay+c4*w*u)+fimpy+den*V*g)^2);
  end
end

%%%%%%%%%%%% differential equations %%%%%%%%%%%%%%%%%%%%
th_prime(1)=(mimp+mfk-m*g*l*sin(th(2))+den*g*V*l*sin(th(2)))/(m*l^2+ja);
th_prime(2)=th(1);

% outputs
F1=fimpc;       % resultant impact force
```

```
F2=mfk/l;          % resultant impact pressure
F3=den*g*V;     % Buoyancy
end
```

2. Solve differential equations of spherical body impact

```
clc
clear
clf
% set initial conditions
lag=0.005;
initial=[0 0.5];
tspan=0:lag:10;

% solve dynamic system in time domain
[t,n_q]=ode45('sphere_stretching',tspan,initial);
figure(1)
subplot(211)
plot(t,n_q(:,2)),xlabel('t(sec)'),ylabel('\theta(rad)'),title('Response Displacement of sphere')
subplot(212)
plot(t,n_q(:,1)),xlabel('t(sec)'),ylabel('\omega(rad/s)'),title('Response Velocity of sphere')

F=[];
FI=[];
FII=[];
for i=1:length(t)
   t1=t(i);n_q1=n_q(i,:);
[a,F1,F2,F3]=sphere_stretching(t1,n_q1);
F=[F F1];
FI=[FI F2];
FII=[FII,F3];
end
```

```
figure(2)
plot(t,F),xlabel('t(sec)'),ylabel('F_{impact}(N)'),title('Impact force','fontsize',16)
 figure(3)
plot(t,FI),xlabel('t(sec)'),ylabel('P_{impact}(N)'),title('Impact pressure','fontsize',16)
figure(4)
 plot(t,FII),xlabel('t(sec)'),ylabel('F_{buoy}(N)'),title('Buoyancy','fontsize',16)
figure(5)
te=t;fe=n_q(:,1);
[spe2,fre2]=pwelch(fe,128,[],[],1/lag);
plot(fre2,spe2),title('smoothed power spectrum of response angular
velocity'),xlabel('frequency(Hz)'),ylabel('P_{uu} (rad^{2}/sec)')
```

3. Self-defined function to calculate submerged volume

```
% to calculate the submerged volume of sphere
function V=vol_sph(r,d)
n=100;       % discrete number
ri=linspace(r-d,r,n);
span=d/n;
V=0;
for i=1:n
   rw=sqrt(r^2-ri(i)^2);
   a=pi*rw^2;
   v1=span*a;
   V=V+v1;
end
```

VITA

Name:	Chunyong Nie
Address:	Delmar Systems, Inc., 2424 Wilcrest Dr., Suite 225 Houston, TX 77042
Email Address:	chunyong.nie@gmail.com
Education:	B.S., Naval Architecture and Ocean Engineering Harbin Engineering University, China, July 2008
	M.S., Ocean Engineering Texas A&M University, Texas, May 2010
Experience:	Civil Engineering Department, Texas A & M University Research Assistant for Dr. Niedzwecki, Sep 2008 – Dec 2009
	Delmar Systems, Inc., Houston, TX Staff Engineer, Dec 2009 - current